A Framework for Biosensors Assisted by Multiphoton Effects and Machine Learning

Jose Alberto Arano-Martinez [1], Claudia Lizbeth Martínez-González [1], Ma Isabel Salazar [2] and Carlos Torres-Torres [1,*]

1   Sección de Estudios de Posgrado e Investigación, Escuela Superior de Ingeniería Mecánica y Eléctrica, Unidad Zacatenco, Instituto Politécnico Nacional, Mexico City 07738, Mexico
2   Departamento de Microbiología, Escuela Nacional de Ciencias Biológicas, Instituto Politécnico Nacional, Mexico City 11340, Mexico
*   Correspondence: ctorrest@ipn.mx

Abstract: The ability to interpret information through automatic sensors is one of the most important pillars of modern technology. In particular, the potential of biosensors has been used to evaluate biological information of living organisms, and to detect danger or predict urgent situations in a battlefield, as in the invasion of SARS-CoV-2 in this era. This work is devoted to describing a panoramic overview of optical biosensors that can be improved by the assistance of nonlinear optics and machine learning methods. Optical biosensors have demonstrated their effectiveness in detecting a diverse range of viruses. Specifically, the SARS-CoV-2 virus has generated disturbance all over the world, and biosensors have emerged as a key for providing an analysis based on physical and chemical phenomena. In this perspective, we highlight how multiphoton interactions can be responsible for an enhancement in sensibility exhibited by biosensors. The nonlinear optical effects open up a series of options to expand the applications of optical biosensors. Nonlinearities together with computer tools are suitable for the identification of complex low-dimensional agents. Machine learning methods can approximate functions to reveal patterns in the detection of dynamic objects in the human body and determine viruses, harmful entities, or strange kinetics in cells.

Keywords: optical biosensors; photonics; machine learning; nonlinear optics; SARS-CoV-2

1. Introduction

The field of biosensors is highly dynamic, with scientific research advances that have mainly flourished in the last decades. Numerous biosensors have been developed for nanotechnology, engineering, molecular biology, computer, and optics [1]. In general, there are three types of biosensors: electrochemical, optical, and piezoelectric; each kind has its own method for transducing signals [2]. Nanoscale functions have been shown to be attractive for manufacturing biosensors [3].

A biosensor is a tool with the ability to detect and determine biological expressions in an environment [4]. This involves a biorecognition fragment for a detailed union and specifies the target molecules (enzymes, antibodies, proteins, cell receptors, toxins, DNA, pharmacists, etc.) [5]. Due to the powerful optical characteristics of semiconductors, they have provided great sensitivity and repeatability for integrated photonic biosensors based on silicon [6]. The performance of the optical sensors in semiconductor platforms may be impacted by two-photon absorption and free carrier dispersion, even if silicon offers optical advantages [7]. Therefore, different scientific groups have oriented their work to design other low-cost materials with advanced characteristics for developing optical biosensors [8].

Optical biosensors outperform standard analytical techniques by allowing real-time, label-free detection of biological and chemical compounds in a highly sensitive, selective,

and cost-effective way [9]. Optical biosensors have been developed for detecting optical signals related to analytes via biocatalytic or bio-affinitive processes [10]. They are categorized according to the mechanism for biosensing, which can be refraction, reflection, Raman scattering, infrared emission, fluorescence, chemiluminescence, absorption, dispersion, or phosphorescence [11].

Optical biosensors can be assisted by plasmonic effects in order to easily identify a virus confirmed by molecules in exhaled air, or droplets such as those represented by nasopharyngeal swabs and saliva [12]. In essence, plasmonic detection techniques act as a viral pre-screening tool to enable the detection of infected individuals [13]. Biosensors have demonstrated their ability to detect viruses in human blood: an example is dengue [14] or chikungunya [15].

Surface plasmon resonance (SPR) has become the most sensitive label-free technique for the detection of various molecular species in solution, and it is of great significance in drug, food safety, and biological reaction studies [16]. SPR excitations are the result of free electron density oscillations and the interaction of electromagnetic waves between dielectric and metal film surfaces; the collective electronic excitations are the fundamental mechanism behind SPR experiments [1]. The reflected light in SPR systems is significantly reduced when the evanescent wave and the surface plasma wave produced by light resonate.

SPR technology has been utilized to produce biosensors for a variety of uses, including plasmonic detectors, optical polarization encoding, sensing technologies, and bio-photonic sensors [17]. SPR has been employed in several biosensor applications because it is highly sensitive to the refractive index of materials nearby [18]. The oscillation of free electrons in the conducting band of the metal is known as surface plasmons. They can only be excited by a polarized wave that is orthogonal to the plane of incidence and the direction of propagation of the surface plasmons [19]. Additionally, remarkable discoveries have been reported for biosensors based on the Raman effect, which is an inflexible shift in radiation frequency caused by optical light in vibrating molecules [20].

Plasmon-based technologies, such as SPR biosensors, have outstanding performance and versatility, and they are one kind of biosensor that is able to detect COVID-19 [21]. An SPR biosensor is capable of completing a reliable COVID-19 test in a matter of minutes compared to other long PCR or antigen tests that patients must perform in medical centers or hospitals [22]. Therefore, SPR-based techniques attract attention for developing biosensors. The detailed processing in SPR simply involves excitation of the coupled-resonator optical-waveguide at a fixed wavelength and imaging of coupled-resonator optical-out-of-plane waveguide's elastic light-scattering huge factor [23]. The method can make use of a discontinuous transition of the coupled-resonator optical waveguide (CROW) eigenstate excited at a fixed laser wavelength in response to a slight change inside the coating refractive index [24].

Single protein detection has been achieved using several label-free optical techniques, including two with imaging capabilities. One involves heating a protein solution with a laser in an indirect manner while the change in the solvent's refractive index is recorded. Interferometric scattering is the base of another technique [25]. The typical method for detecting the scattering light of plasmonic nanoparticles is based on scanning the spectra of nanoparticles using dark-field microscopy, which is time-consuming, laborious, and the small capacity of the sample regularly acts as a limitation [26]. On the other hand, surface-enhanced Raman scattering (SERS) methods are also assisted by SPR effects provided by specific metal nanoparticles such as their main component [20]. The double recognition biosensor SERS is an effective way to measure a variety of biological agents in the laboratory [27].

Biosensors based on bimetallic nanostructures have demonstrated high sensitivity in the detection of different substances, acting as an alternative for use [28]. In addition to their portability and high detection efficiency, some biosensors based on SERS can be reused more than three times when replacing the thread of the DNA substrate and washing the microfluidic device again [29]. Recently, several SERS substrates have been developed

for biosensor applications with a high signal improvement for superimposed plasmonic fields. SERS is very attractive as an alternative method for detecting quantitative and co-multiplexed DNA because it can generate specific molecular oscillation spectra [30].

SERS-based methods have had a high impact on biomolecular analysis due to several factors, such as the fingerprint signal from the SERS nanotag and the stability [31]. As a rule, when a laser illuminates nanoparticles immobilized with the Raman reporter molecule, a local hotspot is initiated, and the Raman signal intensity of the reporter molecule is amplified by several orders of magnitude [32]. So far, research papers have been published demonstrating the potential of SERS-based methods for detecting sensitive and multiplexed biomarkers [33]. The dispersion of the cross-section spectrum shows a peak whose position also depends on the thickness of the biomolecular layer of the nanoparticles. The dependence of the cross-section spectra and the corresponding maximum changes in the thickness of the biomolecular layer are presented by a dispersing effect. Compared with the peaks of the absorption and dispersion spectra, the position of the peak of the dispersion spectrum is more sensitive to changes in the thickness of the biomolecule layer. The peak dispersion change can be about 8 nm, while the saturable absorption can be 2.5 nm [34]. In previous investigations, it has been pointed out that the optical characteristics of cadmium telluride nanorods have a better property under laser excitement with the absorption coefficient of two-photon absorption of 12.0×10^{-10} m/W at 100 μJ. Applications of cadmium telluride nanorods seems to be promising for the next-generation nonenzymatic biosensors and memory devices [35]. However, nonlinear optical (NLO) properties of semiconductors are limited by power level requirements. Nonlinear semiconductors are designed to exhibit high nonlinearity in refraction without effects associated with two-photon absorption; this method allows waveguides to operate at low power levels. For example, it has been indicated that silicon photon waveguide biosensors can detect variations in the transmission spectrum at 1550 nm of the urine glucose concentration with the evaluation of the refractive index [36].

It must be highlighted that NLO processes have opened up a variety of options for improving biosensors. There are many important factors to consider when designing nonlinear biosensors, including the refractive index of the optical media being used [37]. In particular, optical biosensors based on photonic crystals have been reported for detecting the concentration of the SARS-CoV-2 pathogen in water [38].

Moreover, in view of the need to overcome these issues, two branches of artificial intelligence (AI): machine learning (ML) and soft computing, have achieved a notable improvement in several research fields by providing agility and efficiency in different applications. Soft computing is an approach that incorporates the uncertainty and imprecision inherent to real world, inspired by systems in nature, mostly the human brain. Thus, a main process in these techniques is learning; machine learning, then, is related to the capability of a machine to infer an approximate solution from past data or to discover patterns and rules from unknown data.

In view of all these points, we analyzed different panoramic opportunities for optical biosensors based on NLOs for the detection of SARS-CoV-2. In this direction, we highlight how different NLO applications assisted by ML have increased their efficiency and speed to carry out tasks assigned to advanced algorithms with a potential for their use in sensing performance.

2. SARS-CoV-2 Biosensors

Compared to SARS-CoV and Middle East respiratory syndrome coronavirus, SARS-CoV-2 has been shown to be far more contagious [39]. The virus, also known as SARS-CoV-2, has had a significant negative impact on the environment and mankind, increasing mortality rates and causing significant economic losses around the globe [40]. In the years 2002 to 2003, the severe acute respiratory syndrome (SARS) was spread by SARS-CoV-2, a single-stranded RNA virus from the genus Beta coronavirus [41]. In 2021, RNA SARS-CoV-

2 was frequently detected on surfaces in the medical environment, even in adaptive and unrelated sewage [42].

Coronavirus disease (COVID-19) outbreaks in several communities have compelled governments worldwide to enact stringent controls such as blockades, border closures, and widespread screening [43]. The SARS-CoV-2 virus is compatible with the coronavirus family with single-stranded gene RNA and surface proteins such as membranes, envelopes, nucleocapsids, and spikes [44]. Cryo-electron microscopy was utilized to establish the structure of the SARS-CoV-2 spike glycoprotein, which was then used for the creation of cell-specific vaccinations [45].

The symptoms of being infected by the SARS-CoV-2 virus can be varied; some symptoms are coughing, discomfort, and fever [46]. Several techniques are available for rapid measurement of antigen levels from both nasopharyngeal secretions and saliva, providing fairly satisfactory duplication of molecular assay results [47]. When performing the standard diagnosis, RNA extraction of the nasopharyngeal swab is required, followed by quantitative reverse transcription PCR (RT-QPCR) [48]. In recent years, some of the investigations have been focused on the design of optical biosensors for the efficient and rapid detection of the SARS-CoV-2 virus. The recognition elements of optical biosensors can be divided into aptamers, molecular imprint polymers (MIPs), and antibodies [49]. Wenjuan and his colleagues created the first unique microfluidic biosensor using Fresnel reflection for the detection of SARS-CoV-2 without a label that is quick, simple, and sensitive [50].

In order to identify the SARS-CoV-2 virus, optical biosensors can generate several wavelengths and collect data on heart rate, nitric oxide levels, pulse oximetry, and kidney function [51]. Courtney and colleagues created a successful biosensor with the ability to detect nucleic acids and with the option to improve with high convergence and mismatch [52]. Silicon nitride low-loss photonic wires have been used in the optical transmission waveguide devices to develop a complementary metal-oxide semiconductor compatible with the plasma-enhanced chemical vapor deposition process [53]. Ebola, HIV, and norovirus viruses have been detected by optical biosensors based on resonators, optical biosensors based on the waveguides, photonic biosensors based on crystals, and fiber-based optical biosensors [54]. In the latest investigations, the possibility of detecting the COVID-19 virus with a low 0.22 pm detection limit has been reported and the difference between SARS-CoV of the SARS-CoV-2 was distinguished by a plasmonic sensor [55].

One of the most intriguing and extensively researched devices is one made by utilizing surface nanopatterning technology. Nanopattern subwavelength characteristics promote actions such as guided mode resonance [56], SERS [56], or localized SPR [57]. Those structures make it possible to identify light interactions with certain biological analytes at the sensor surface effectively.

In order to increase the sensibility of sensing materials, photonic crystals have been proposed as periodic arrangements of dielectric materials built in an area of incoming radiation [58]. Similar to the bandgap in semiconductors, they have a photonic bandgap where it is forbidden for some wavelengths to pass through their structure [59].

In the past two decades, integrated photonic biosensors have become the focus of significant study because they can be miniaturized and can effectively detect relatively low concentrations of analytes in real time [60]. According to Srivastava and colleagues, the magnified changes caused by the conversion to photonics are sensitive to changes in the refraction index of the sensing medium; this makes the nanostructures an excellent choice for a biosensor [61]. Most of the photonic integrated sensors employ the concept of evanescent field detection, where the analyte adheres to a bioreaction layer on the surface of the wave guide and interacts with the evanescent field of the guided wave [62]. The initial displacement in particular biosensors may be increased by about four orders of magnitude by utilizing preselection to choose the polarization and postselection to create destructive interference [63]. This signal enhancement approach can simplify the optical components and lower the cost of the sensor device in addition to measuring the spin-dependent splitting in biosensors [64]. Furthermore, due to its distinct optical characteristics, the

photonic spin Hall effect has generated a lot of study in recent years [62]. On-chip resonant or interferometric devices are used to translate changes in the optical phase, which cannot be detected directly, into changes in the optical power [63].

SPR biosensors are particularly effective in detecting bacterial viruses and pathogens among various biodetection methodologies [65]. By using this method, slow PCR and ELISA techniques are avoided. The first investigation by Wrapp and colleagues focused on the high affinity of the SARS-CoV-2 protein with ACE2 [66]. More recently, a unique localized SPR biosensor with the twin capabilities of plasmonic photothermal and sensing transduction was presented [67].

A very efficient technique for rapid detection is worth mentioning. It is without labels and is precise for a variety of pathogens and viruses that have been based on SPR [68]. In the past, it was asserted that an SPR-based biosensor could recognize the feline calicivirus in about 15 min [69]. In the same way, a very similar discovery was obtained for human enterovirus 71 (EV71) [70]. Research has found different forms of rapid and precise detection of COVID-19, and nanophotonic biosensors have been developed [67]. An SPR optical biosensor with a gold nanoparticle coating was successfully developed by researchers as a COVID-19 detection device [71]. For the potential detection of coronavirus illness, different optical biosensors with localized SPR have been presented [72].

It is possible to improve SPR platforms of localized SPR devices for the identification of COVID-19 [73]. Ren-min and Oulton's study demonstrated the use of the nanolaser method as a biological optical detector [74]. For monitoring small chemical molecules, photonic glass fiber biosensors have been integrated by using porous silicon structures [75]. In order to find comparative chemical compounds, photonic crystal fiber biosensors based on a porous silicon have also been described [76]. Typically, the SPR biosensor is employed to identify biological or chemical materials [77]. Previous experiments demonstrated the potential of SPR biosensors for viral detection without real-time labels [78]. An overview of representative works in this area is shown in Table 1.

Table 1. Representative optical biosensors papers for the detection of SARS-CoV-2.

Journal	Detection Limit	Analyte Types	Optical Effect	Year	Reference
Biosensors and Bioelectronics	2 μL	The genes of S, N, and Orf1ab	Evanescent wave fluorescence	2021	[79]
Talanta	1.0 mg/mL	Immunoglobulins (G, M, and A)	Colorimetric	2021	[80]
Talanta	12.5 ng/mL	IgG antibody	Evanescent wave fluorescence	2021	[81]
Sensors and Actuators B: Chemical	1 and 0.033 ng/mL	Spike 1 protein	Fluorescent bifunctional	2022	[82]
Chemical Engineering Journal	43.70 aM	RNA-dependent RNA polymerase gene	Electrochemiluminescence	2022	[83]
Environmental Science: Nano	32.80 aM	RNA-dependent RNA polymerase gene	Electrochemiluminescence	2022	[84]
Biosensors and Bioelectronics	2.75 fM	Spike protein, matrix protein, envelope protein, and nucleocapsid	Colorimetry G-quadruplex	2020	[85]
Virology	-	Nucleocapsid protein	Luminescence	2021	[86]
Talanta	59 aM	Nucleic acid	Electrochemiluminescence	2022	[87]
Chemical Engineering Journal	7.8 aM	RNA-dependent RNA polymerase gene	Electrochemiluminescence	2022	[88]
Viruses	50 μg/mL	Angiotensin-converting enzyme 2	Bioluminescent	2021	[89]
Cold Spring Harbor Laboratory	50 μg/mL	Angiotensin-converting enzyme 2	Bioluminescent	2020	[90]
Physica Scripta	1020 nm/refractive index unit (RIU)	Pathogens of SARS-CoV-2	Refractive index	2022	[38]

Table 1. *Cont.*

Journal	Detection Limit	Analyte Types	Optical Effect	Year	Reference
Sensors and Actuators B: Chemical	-	Spike protein	Optical interferometry	2021	[91]
SSRN Electronic Journal	833.33 nm/RIU	Spike glycoprotein	Refractive index	2022	[92]
Talanta	514 aM	spike protein, nucleocapsid protein, the RNA-dependent RNA polymerase gene	Electrochemiluminescence	2022	[93]
Sensors	0.1 fM	Open reading frames 1ab gene	Electrochemiluminescence	2022	[94]
Talanta	0.22 pM	Spike protein	Refractive index	2021	[55]
Analytica Chimica Acta	48 ng/mL	SARS-CoV-2 spike antigen	Colorimetric	2021	[95]
Analytica Chimica Acta	1.0×10^{-6} RIU	Spike protein receptor-binding domain	Fresnel reflection	2021	[96]
2021 IEEE 15th International Conference on Nano/Molecular Medicine & Engineering (NANOMED)	114.07 nm RIU^{-1}	COVID-19 virus detection by delivering quick, dependable results	Refractive index	2021	[22]
Scilight	~106 virions/mL	SARS-CoV-2 proteins (membrane, envelope, and spike)	Colorimetric	2021	[97]
Biosensors and Bioelectronics	17 aM	SARS-CoV-2 RNAs with single molecule sensitivity	Electro-optofluidic	2021	[98]
Biosensors and Bioelectronics	-	Nucleic-acid-based testing	Colorimetric	2021	[99]
Journal of the American Chemical Society	-	Spike antigen and cultured virus	Luminescent	2022	[100]
Biosensors and Bioelectronics	370 vp/mL	SARS-CoV-2 virus particles in one step	Nanoplasmonic resonance	2021	[101]
ACS Applied Materials & Interfaces	0.21 fM	RNA-dependent RNA polymerase gene	Electrochemiluminescence	2021	[102]
In vitro models	1 μg/mL	S protein of SARS-CoV-2	Colorimetric	2022	[103]
Biosensors and Bioelectronics	3 copies/μL	Two regions in nucleocapsid gene (N1 and N2 genes)	Fluorescence polarization	2021	[104]
Biosensors and Bioelectronics	1 mg/mL	Immunoglobulins G and M	Optical/chemiluminescence	2021	[105]
Viruses	100 pM	Spike proteins, nucleocapsid proteins	Fluorescent	2022	[106]
Microchimica Acta	4.98 ng/mL^{-1}	Angiotensin-converting enzyme 2	Colorimetric	2021	[107]

From Table 1, we can observe different optical and photonic biosensors that perform the function of detecting SARS-CoV-2. The advantage of using optical biosensors is the ease of use. The optics tools have demonstrated with some applications the ability to improve the resolution, speed, and efficiency of biosensors. Moreover, biosensors based on nonlinear absorption, Raman dispersion, or SPR can present advantages in biosensing regarding the potential for multiphoton effects. Table 2 presents these characteristics for detection of SARS-CoV-2. Table 1 describes biosensors assisted by optical effects, while Table 2 mentions biosensors that are related to multiphoton effects.

Table 2. Representative multiphoton biosensors papers for the detection of SARS-CoV-2.

Journal	Detection Limit	Analyte Types	Optical Effect	Year	Reference
IEEE Sensors Journal	2.5 ng/mL	Nucleocapsid protein	Plasmonic fiber optic absorbance	2021	[108]
Biosensors	0.047 μg/mL	SARS-CoV-2 pseudovirus	Surface plasmon resonance	2022	[109]
Biosensors and Bioelectronics	0.77 fg/mL^{-1}	Spike protein	Raman scattering	2021	[110]
Sensors and Actuators B: Chemical	50 and 10 pfu/mL	Angiotensin-converting enzyme 2	Raman scattering	2022	[111]
ECS Meeting Abstracts	-	Antibodies to SARS-CoV-2	Surface plasmon resonance	2021	[112]
Analytical Chemistry	45.6 to 86 ng mL^{-1}	Nucleocapsid protein	Plasmonics	2022	[21]
Biosensors and Bioelectronics	2 ng/spot	spike S1, spike S1 S2, and the nucleocapsid protein	Fluorescent plasmonics	2021	[113]
Sensors	4.2 μg/mL	Spike protein	Photonics	2021	[114]
Analyst	12 fg mL^{-1}	Spike S1 protein	Surface plasmon resonance	2022	[115]
Biomedical Vibrational Spectroscopy 2022: Advances in Research and Industry	-	Spike protein	Raman spectroscopy	2022	[116]
Plasmonics	152°/RIU	Spike proteins, membrane proteins, envelop proteins, and nucleoprotein	Surface plasmon resonance	2022	[117]
Sensors	250 μg/mL	Spike (S1 and S2) proteins	Surface plasmon resonance	2021	[118]
IEEE SENSORS 2021	8.34 ng/mL	Spike protein	Surface plasmon resonance	2021	[119]
Biosensors and Bioelectronics	1 μg/mL	Nucleocapsid antibody	Surface plasmon resonance	2022	[120]
AIP Advances	54.04 RIU^{-1}	Spike glycoprotein	Surface plasmon resonance	2021	[67]
Analytical Chemistry	-	Spike surface glycoprotein	Surface-enhanced infrared absorption	2021	[13]
Matter	10 PFU/mL	Spike glycoprotein and membrane protein	Raman scattering	2022	[121]
ACS Applied Nano Materials	200 PFU/mL	Spike proteins	Raman scattering	2022	[122]
ACS Nano	0.22 pM	RNA-dependent RNA polymerase	Localized surface plasmon resonance	2020	[123]
Analytical Chemistry	-	Angiotensin-converting enzyme 2	Surface plasmon resonance	2020	[124]
Biosensors and Bioelectronics	150 ng/ml	Detect SARS-CoV-2 nucleocapsid proteins	Localized surface Plasmon resonance	2022	[125]
Analytical Methods	200 μL	Spike and nucleocapsid proteins	Surface plasmon resonance	2021	[126]
Sensors & Diagnostics	10 RU	Spike protein	Surface plasmon resonance	2022	[127]
Biosensors and Bioelectronics	2×10^{11} particles/mL	Nucleocapsid phosphoprotein gene	Raman scattering	2022	[128]
BioChip Journal	1.02 pM	Antibodies against nucleoprotein	Surface plasmon resonance	2020	[129]
Nanoscale Advances	4.5 fg/mL^{-1}	SARS-CoV-2 spike protein	Raman scattering	2022	[130]

Table 2. *Cont.*

Journal	Detection Limit	Analyte Types	Optical Effect	Year	Reference
Biosensors and Bioelectronics	0.08 ng/mL	SARS-CoV-2 spike protein	Localized surface plasmon resonance	2020	[131]
Analytical Chemistry	4 mg/mL	SARS-CoV-2 spike protein	Surface plasmon resonance	2021	[132]
Plasmonics	1×10^{13} per m^2	Thiol-tethered DNA of SARS-CoV-2	Surface plasmon resonance	2021	[133]
Talanta	0.046 ng/mL	SARS-CoV-2 spike protein	Raman scattering	2022	[134]
Talanta	100 pg/mL^{-1}	Measurement of SARS-CoV-2 antibody	Photonic resonator absorption	2021	[135]
Talanta	37 nM	SARS-CoV-2 spike glycoprotein	Surface plasmon resonance	2021	[136]

3. Biosensors Assisted by Machine Learning

As was mentioned before, ML is a subfield of artificial intelligence (AI) that provides another way to gain insight into complex data [137]. ML uses computational systems to simulate human learning and gives the algorithm the ability to recognize and acquire knowledge of the environment to improve performance [138]. Complex biological systems are naturally compatible with ML methods that can effectively detect hidden patterns [139]. Predictive information multiplexed can be obtained by increasing analysis of responses in a sequence [140].

ML-assisted biosensors can be used in complex environments and without having the characteristics of a laboratory study [141]. A typical process is shown in Figure 1. Raw data acquired by a biosensor are preprocessed (data filtering, missing values, segmentation; normalization is also carried out early in this step to homogenize scales or data types) according to the nature of the data. Features or characteristics are then extracted to represent the differences in the data and also to reduce the amount of data. This features set X is called features space. Dimensionality reduction of X is carried out to select the most significant variables and decrease complexity. It is worth mentioning that the quality of data is relevant. ML learns from the sample; if there is noise or the sample is not significant, overfitting will occur and the performance of the algorithm will be poor.
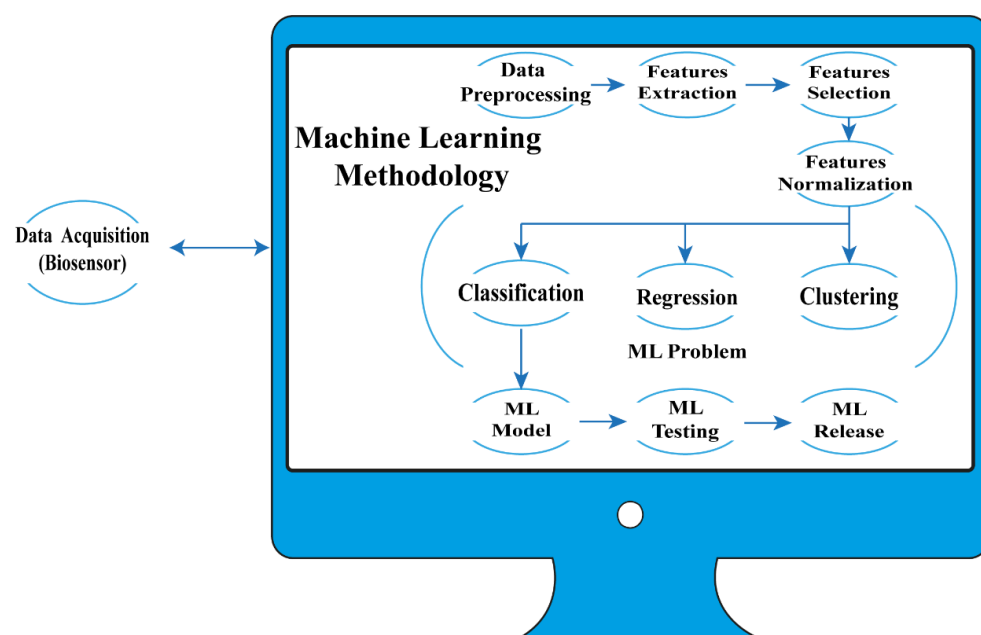

Figure 1. Biosensors assisted by ML.

In general, three types of problems can be approximated with ML: classification, regression, and clustering problems. Dimensionality reduction by itself is also considered a type of problem solved by ML, and clustering is commonly a previous step in a classification problem.

According to the nature of X, the learning process in ML is divided into two main categories: supervised and unsupervised learning (Figure 2). When the inputs X are known or labeled, the learning process is called supervised. The objective in a problem of classification or prediction (regression) is to approximate a function $f(X) = Y + \varepsilon$, to approximate the output or labels Y with an error ε. In this learning process, ML methods use a subset of X to train a model. Once the model has been trained, it is tested with the rest of the available data. This step is repeated until the approximate function reaches an error goal; then, the model is released to classify or predict new unknown data. A balance among two types of error should be taken into account: bias, which is the result of the assumptions of data behavior in learning the objective function, and variance, which indicates how different the function approach will be according to the training dataset used. Different algorithms are used for these learning processes; some of them are usually applied to data analysis, such as linear regression. Other algorithms categorized in ML are logistic regression, support vector machines (SVM), naïve Bayes, decision trees, and k-nearest neighbors (KNN). On the other hand, the learning process is called unsupervised when X is not labeled; here, the objective is to discover the patterns in the data to generate clusters with similar features. The most popular algorithm for this learning process is k-means.
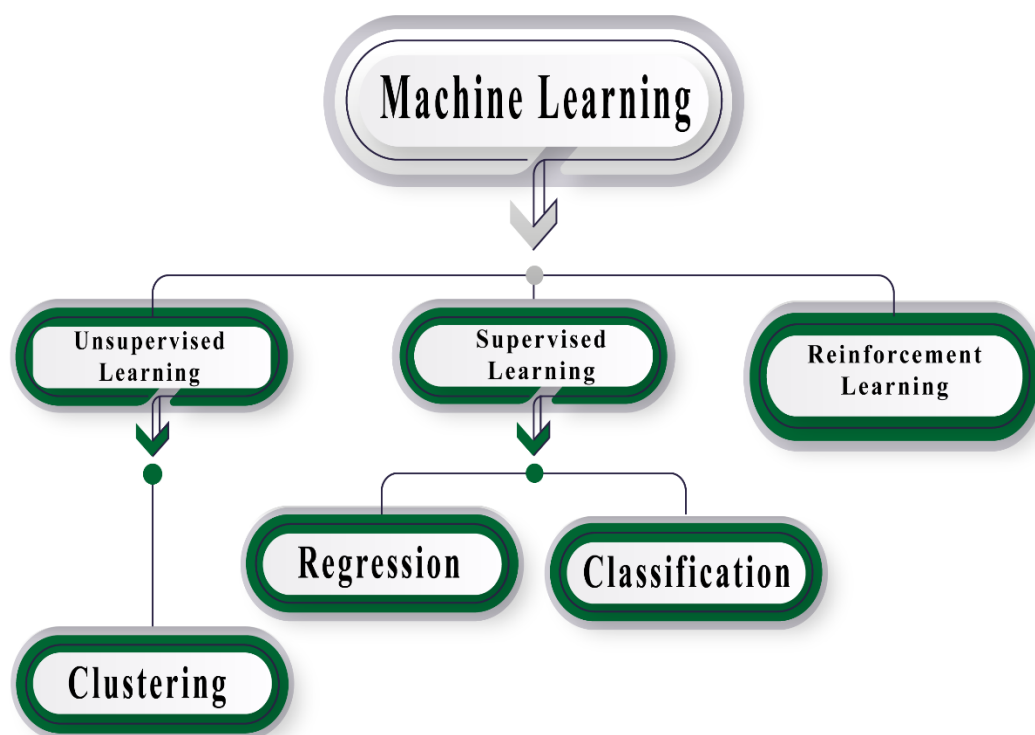
Figure 2. ML categories according to the nature of the features space.

Soft computing algorithms are those strictly inspired by nature, for instance, artificial neural networks (ANNs), fuzzy systems, genetic algorithms, swarm algorithms, and ant colony optimization algorithms. Soft computing methods are especially useful for optimization problems; in this sense, ANNs and other ML algorithms optimize the error of the objective function.

The acquisition of information can be enhanced by automatic learning tools [142]; in this direction, optical biosensors have made a great contribution to medicine by being non-invasive and ultrafast. On the other hand, ML can improve these results, simplifying the

analysis of the raw data from the biosensors output, to approximate a solution to different problems. For instance, (a) classification, for detection or diagnosis and treatment decisions support; (b) regression, to predict and prevent non-desirable events; and (c) clustering, to find groups of data that share features, such as symptoms, characteristics of a disease, or a strange behavior in different scales (e.g., enzymes, hormones, cells, organs, systems, and the whole body). The signals provided by the optical biosensor can be monitored in real time to outflow tract constructions that are useful in ML methods [143].

For instance, a supervised automatic learning method with optimized characteristics has been implemented to consider the effects of decreased enzymatic activity [144] or glucose in a sample [145]. ML regression statistical models have been applied to estimate the current response of a second-generation amperometry glucose oxidase biosensor [146].

Neural Networks in Biosensors

An artificial neural network (ANN) consists of a node layer that has an input layer, one or additional hidden layers, and an output layer [147]. Every node or artificial nerve cell connects to a different node and has acceptable weights and thresholds [148]. Once a private node output exceeds a threshold, that node is activated and sends data to a consequent layer within the network [149], as illustrated in Figure 3.
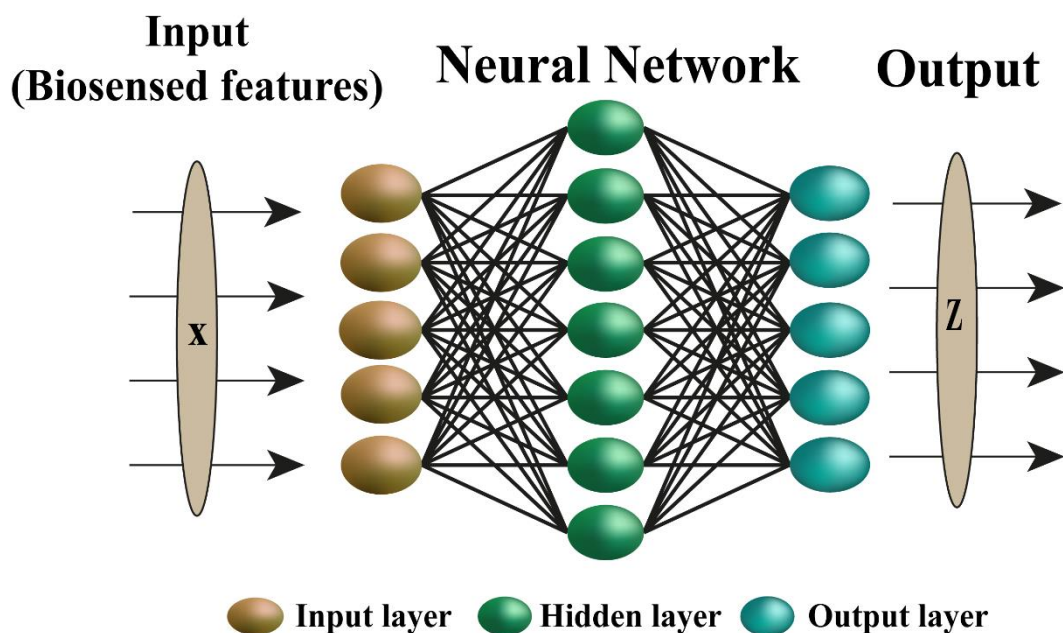

Figure 3. ANN common structure.

There is research demonstrating the improvement in the use of neural networks (NNs) in the enhancement of signal processing. In fact, it has been found that the combination of spectrum in spectrograms is an effective way to classify strong signs of biosensors [150]. In biosensors, pathogen agents and neurons associated with the disease have an important value. In recognition of the excellent classification capacity of the convolutional neuronal network model, it is also possible to perform the classification of a disease using biosensors [151]. An example of this is Mennel and colleagues, who conducted an image detection study applying an ANN [152].

In recent years, optical biosensors have received attention from the scientific community due to their advantages, such as detection with high sensitivity [153]. Different fluorescent materials such as quantum dots [154] and fluorescent microspheres have been used [155]. A technique to measure the fluorescent signal is excitation using a sensitive fluorometer; this determines the concentration of the bacteria. Instead of determining the target bacteria concentration, fluorescent bacteria can also be counted directly. NNs algorithms fulfill the function of processing the images obtained from fluorescent bacteria.

NNs processing manages to calculate the amount of fluorescent points faster to determine the target bacteria [156].

4. NLO Processes Analyzed with ML

Prediction of nanoscale functions in multiphoton experiments is attractive for describing different NLO effects [157]. Analysis of third-order NLO techniques by ML has conjointly progressed throughout the last decade [158], considering all-optical functions for sensing and signal processing by ML [159]. There has been growing interest in generating pulses with repetitive frequencies on the order of gigacycle per second with the assistance of deep learning [160]. Measurements of ultrafast optical pulses for sensing represent challenges for scientific research in ML methods [161].

A roadmap of representative research on NLO applying ML methods is shown in Figure 4. ML for studying chaotic nonlinear dynamics [162], self-tuning for mode-locked lasers [163], laser optimization [164], and the measurement of extremely short pulses; it should be noted that their duration is much shorter than the response times of most photodetectors [165]. Ultrashort pulses are widely used to monitor chemical reactions, control THz radiation, cipher pulses for communication, and form optical pulses [166]. ML has been used to measure time unit pulse duration using time unit detectors [167].
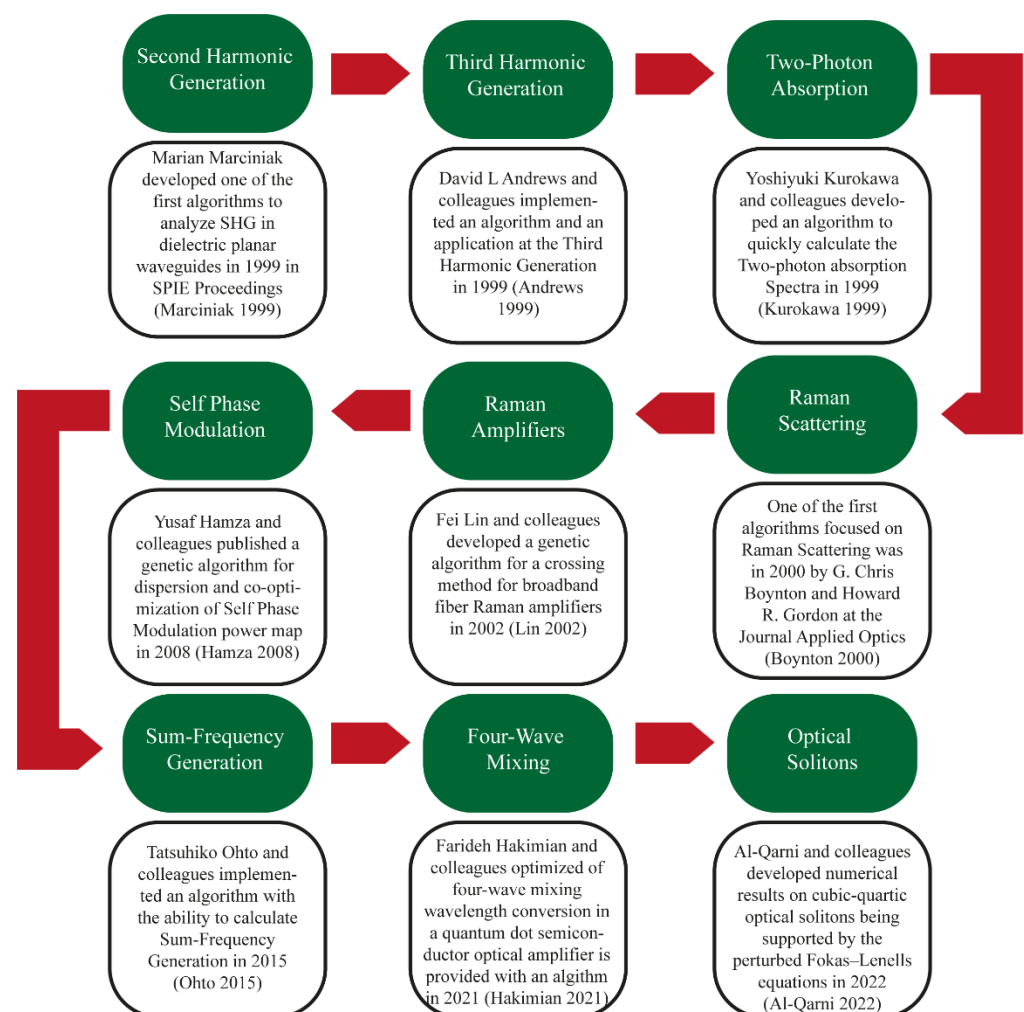
Figure 4. Roadmap of investigations based on NLO processes assisted by ML and soft computing [168–176].

The most promising methodology to atone for nonlinearities in single channel systems is the digital backpropagation algorithm, which works by digitally modeling the fiber chan-

nel [177]. The disadvantages of this method are the high procedure complexity of the time period application and also the impossibility of accurately modeling the channel because of the looks of random parameters [178]. For these reasons, analysis on nonlinear compensation is currently centered on computing techniques [179]. Extraordinarily short pulses are troublesome to explain due to the massive variety of the parameters concerned [180]. With such systems, small changes in state variables will cause changes in momentum dynamics, which is particularly necessary with ML-based algorithms [168–176] (Roadmap).

4.1. Second-Harmonic Generation

The second-order NLO process in which photons that interact with a nonlinear material "combine" effectively is known as second-harmonic generation (SHG) [181]. SHG, which depends on a second-order NLO difference system, permits specialists to perform non-checking and non-horrendous imaging of tissue structures at the cell level [182]. Currently, when relevant areas in SHG images are detected, further medical actions can be proposed [183]. However, no simplifying assumptions or analytic solutions have been found to obtain SHG's accurate spatial phase distribution [184]. The core measures employed in SHG simulation continue to be numerical techniques such as the split-step method and the Fourier-space algorithm [185].

The variation that uses SHG is simple for frequency-resolved optical gating (FROG). In fact, the pulse-shaping community frequently employs SHG FROG in nonlinear spectroscopy and coherent anti-Stokes Raman diffusing to discover potential extremely complex beats [186]. Furthermore, due to well-known trivial ambiguities, it has been mathematically demonstrated that all pulses may be uniquely predicted by SHG FROG [187]. More recently, a nonlinear time-domain finite difference method was developed by modifying Yee's algorithm into a potent modeling technique that can take nonlinear phenomena such as second- or third-harmonic generation into consideration [188]. Intrinsic signals can be viewed as label-free using a nonlinear mode of multiphoton excitation called SHG [189]. Qun and colleagues have applied the SHG effect with the help of ML methods to develop images of the samples of thick heart tissue [190].

Since the discovery of quartz's piezoelectricity more than a century ago, the need for effective materials for novel piezoelectric and NLO applications has steadily increased. Although piezoelectric materials are supposed to have the highest electromechanical coefficients, excellent SHG characteristics are crucial for NLO applications [191]. ANNs speed up optimization of genetic algorithms and store sample information that can be easily generalized to other samples with minimal additional training [192]. Hall and colleagues developed an impartial and efficient algorithm to quantify the images of SHG in tissues [193].

The continuous wave laser radiation in the UV range is often realized due to nonlinear effects such as four-wavelength mixing or SHG [194]. ANNs speed up optimization of genetic algorithms and store sample information that can be easily generalized to other samples with minimal additional training [195]. Deep-ultraviolet NLO crystals for current and upcoming basic research and technology requirements, a succinct SHG output wavelength, and a frequency conversion ratio are crucial [196]. SHG coefficients are shown to be inversely related to the band gap via the sum-over-states formula [197].

By using second-order NLO differential elements in SHG imaging, specialists can conduct label-free, non-destructive studies of tissue architecture [198]. Up to the current date, there is no published study that suggests using ML to instruct users about adjustable NLO vulnerability and exchanging behavior for sensing [199].

4.2. Nonlinear Optical Absorption

The optical absorption coefficient of a material that depends on irradiance is known as nonlinear optical absorption [200]. The absorption coefficient disappears at the dissipation intensity. In other cases, absorption is observed at low intensities, but the absorption coefficient increases or decreases at high intensities [201]. In order to address nonlin-

ear tomographic absorption spectroscopy issues, Deng et al. looked deeper into how well other complicated deep ANNs, such as deep belief networks and recurrent ANNs, performed [202]. It is advantageous for photonic computing applications because of its straightforward design, very quick operation, and high NLO coefficient [203]. However, only basic investigations of direct absorption-spectroscopy-based deep learning algorithms for nonlinear tomography issues have been performed [204]. Only temperature or particle concentration may be reconstructed using the deep learning network provided [202].

4.3. Optical Kerr Effect

The Kerr nonlinearity has an NLO impact when light induces a change in the refractive index by different physical mechanisms such as electronic polarization or molecular orientation. It can be portrayed as an induced birefringence caused by optical irradiance and is dependent on the square of the electric field that can be supervised by ML [205].

The Kerr law of nonlinearity emerges when a light wave in an optical fiber meets nonlinear responses because of nonharmonic mobility of electrons trapped in molecules produced by an external electric field [206]. Solli and colleagues observed for the first time the rogue waves in one-dimensional settings in the field of optics [207]. Chalcogenide glass, which has a very strong Kerr effect and reacts right away to electrical stimulation, was employed by Gopalakrishnan and colleagues to obtain experimentally meaningful values for the above described [208]. Jhangeer and his colleagues developed an algorithm capable of obtaining wave solutions of exact paths of complex nonlinear partial differential equations [209]. This is achieved by improving the perturbative nonlinear Schrödinger equation with the nonlinear Kerr effect, which is an important equation for soliton testing in optical communication networks.

4.4. Sum Frequency Generation

A second-order NLO mechanism called sum frequency generation (SFG) works by annihilating two input photons with each frequency ω_1 and ω_2 while simultaneously generating one photon with frequency ω_3 [210]. When imaging self-assembled thiol monolayers on gold using the SFG spectroscopic method, ANNs are utilized as a substitute for chemical identification [211]. ANNs are also particularly helpful for solving issues when it is difficult or impossible to provide realistic physical or mathematical models [212].

4.5. Self-Phase Modulation

An NLO result for the interaction between matter and the vectorial nature of light is self-phase modulation (SPM). Due to the optical Kerr effect, a medium's refractive index changes when an ultrashort light pulse passes across it [213]. Since NN can adaptively correct for distortion, NN-based digital signal processing has been researched to account for nonlinear effects in wireless communication systems [214]. Only intensity-modulated direct detection transmission methods have been analyzed for nonlinear distortion correction in optical communication systems. In order to correct for the distorted multilevel optical signal caused by SPM, Shotaro and colleagues suggested a novel nonlinear equalization technique employing NN [215]. Caballero and colleagues developed a method with the ability to estimate signal-to-noise linear ratio and nonlinear ratio considering SPM assisted with an NN [216].

4.6. Raman Amplifiers

The reasonable choice of pump powers and wavelengths is a key element in accomplishing a wanted Raman pick-up profile. This is often a challenging assignment as the relationship between power profile versus pump powers and wavelengths is nonlinear and requires broad numerical reenactments to anticipate [217]. Raman amplifiers have lately attracted fresh interest as a result of their ability to amplify broadband signals by the assistance of ML when used in a multi-pump laser arrangement [218]. In addition, they have reduced noise when using distributed amplifiers and ML [219]. The Raman ampli-

fiers' capacity to arbitrarily set the gain by varying the pump power and wavelength is another distinctive quality improved by ML [220]. This gives optical amplifiers and optical communication systems unprecedented flexibility and capacity for dynamic adaptation by using deep learning techniques [221]. An example is distributed Raman amplifier (DRA), which is an important amplification method in optical communication systems due to its low noise figure and flexible wideband gain obtained by using ML [222]. Raman gain design and analysis have benefited greatly from the successful use of ML in other domains of optical communication in recent years [223].

Optimizing the pump design to obtain the appropriate gain spectrum at the amplifier output is the key research goal of the Raman amplifier [218]. This challenging optimization issue calls for the solution of a set of nonlinear differential equations. Many algorithms have been developed [224], as well as ANN [225] or ML [226] to find a solution to the conflict between the pump setting and the intended spectral gain setting. Currently, an ML strategy has been proposed for single-mode fibers [227] and few-mode fibers [225]. A dataset of hundreds of advantage bends made with erratic pump powers and wavelengths is used to train an NN to consider the relationship between the pump parameters [228].

4.7. Surface-Enhanced Raman Scattering

Molecular polarizability can be used to explain Raman scattering [229]. Electrons and nuclei are shifted when a molecule is put in an electric field [230]. An electric dipole moment is produced in the molecule because of the separation of charged species, and the molecule is said to be polarized [231]. A molecule scatters irradiant light from a source laser in the Raman method, which is a light scattering technique [232]. Most of the scattered light is of the same wavelength as the laser source and hence useless, but a tiny quantity of light is dispersed at various wavelengths and so is beneficial [233].

The molecules can be coherently driven to a state of breath and can then generate signals that are usually of a stronger magnitude than the spontaneous Raman dispersion [234]. This happens when there is a difference between the pump field and the Stokes field in the coincidence in active vibrations of the molecules in the sample [235]. By analyzing NLO effects, a quick and efficient response is required; an example is the impact of amplified spontaneous emission and nonlinear interference reported by Margareth and colleagues [236].

Raman microscopy is another option for label-free imaging; however, because of the poor effectiveness of Raman scattering, neuron imaging with ordinary spontaneous Raman scattering needs a considerable exposure period [237]. Plasmonic materials have been employed to boost the Raman technique's sensitivity. Pengju and colleagues utilized a calculation based on ML to classify the ordinary and extracellular cancer vesicles and parties [238].

SERS, which has sensitivity down to the level of a single molecule, is perfect for multichannel detection [239]. Based on this idea, SERS physiology was very recently developed in order to offer speculative details about nearby cellular metabolites [240] by accumulating time-based SERS spectra constantly. The way the data were processed also had limitations in the original photophysiological trials for SERS. An ML method that is adaptable was proposed by Leong and colleagues [241].

4.8. Summary of Representative Nonlinear Optical Effects Assisted by ML Algorithms

The progress and development of new research in ML has opened up the opportunity to advance new techniques for the collection and interpretation of information in applications in different sciences. By joining the different optical processes to the interpretation of ML data, it opens up a variety of options and applications. The development of biosensors based on optical processes has provided the ability to detect biological agents in different organisms, facilitating their analysis. The study of the NLO processes assisted by ML involves the extraction of the properties that can represent fundamental information for sensitive classifying and segmentation.

NLO processes have been developed for the use of detection of different materials that can be used for improving biosensors. The most used multiphoton process for the detection of the SARS-CoV-2 virus has been Raman scattering; this is due to its advantages in the field of optics. Table 3 shows different NLO processes that are assisted by computer systems.

Table 3. NLO processes assisted by computational methods.

Journal or Conference Event	Application	Optical Effect	Year	Reference
Sensors	Optical biosensors supported by algorithms for rigorous monitoring and control in the identification of bacteria	Light Diffraction	2020	[242]
PLOS ONE	Comparison between Marquardt Algorithm vs. Newton Iteration Algorithm for biomolecular interaction process between antigen and antibodies or receptors	Optical Surface Plasmon Resonance	2015	[243]
Scientific Reports	Improves the image difference between normal tissues and tumors	SHG	2021	[244]
BMC Cancer	An independent predictive measure of metastasis-free survival in patients with invasive ductal cancer	SHG	2020	[245]
SPIE LASE	Enhanced Pulse Extraction Algorithm FROG used for geometry	SHG	2019	[246]
Atmospheric Measurement Techniques	Measures the error between CO and CO_2 by nonlinear absorption and fluctuations in interference coefficients	Nonlinear Absorption	2013	[240]
Journal of Lightwave Technology	A scheme allowing the soliton comb to be determined under a specific pump scan, with an error of <8%, verified by experimental measurements	Optical Kerr Effect	2020	[247]
SSRN Electronic Journal	Tackling the effects of the intra-polarization self-phase modulation and inter-polarization cross-phase modulation	SFM	2022	[248]
Optics Express	Optimizes the pump wavelength	Raman Amplifiers	2020	[249]
Optical Fiber Communication Conference (OFC) 2020	Gains improvements for a few mode fiber amplifiers	Raman Amplifiers	2020	[250]
Spectrochimica Acta Part A: Molecular and Biomolecular Spectroscopy	Detection of quantity of chlorpyrifos in rice.	Raman Scattering	2021	[251]
Food Chemistry	Quantifies the systemic fungicide residues of Benzimidazole (Thiabendazole) in apples	Raman Scattering	2021	[252]
ACS Nano	Performs the measurement simultaneously from gradients, at least eight in vitro metabolites along with different cell lines	Raman Scattering	2019	[253]
2021 IEEE International Conference on Big Data (Big Data)	Improves rapidity in the inspection of the techniques of images of cellular and tissue pathology	Raman Scattering	2021	[254]
2018 Cross Strait Quad-Regional Radio Science and Wireless Technology Conference (CSQRWC)	Sorts different varieties of honey	Raman Scattering	2018	[255]
In Proceedings of the 2021 IEEE 21st International Conference on Nanotechnology	Label-free method for detection of protective anthrax antigens based on SERS	Raman Scattering	2021	[256]

Table 4 shows different applications that improve the analysis of the processes of the NLOs assisted by computer systems. Figure 5 shows the different nonlinear optical effects mentioned in this work, with a sample of SARS-CoV-2 as an example.

Table 4. Publications about NLO processes assisted by ML.

Journal	Application	Algorithm	Nonlinear Optical	Year	Reference
Journal of Lightwave Technology	A standard for optical quality	A new approach to direct-learning-based pre-distortion using ANN	High throughput coherent optical	2020	[257]
2017 International Conference on Orange Technologies (ICOT)	Using a Computer-Aided Diagnosis (CAD) system, stem cells in the stratum basale are studied	Convolutional ANN	Third-harmonic generation	2017	[258]
Optical and Quantum Electronics	Optimizing the wavelength conversion for four-wave mixing in a quantum dot semiconductor optical amplifier	A fresh method based on ANN and genetic algorithms	Four-wave mixing	2021	[176]
IEEE Photonics Journal	Extrapolates helpful characteristics and details from the SERS signal	A novel approach to enhance SERS signals using principal component analysis as an ML approach	Raman scattering	2020	[259]
Applied Optics	Encryption scheme	A fresh nonlinear picture encryption method using the Fresnel transform domain's Gerchberg–Saxton phase retrieval algorithm	Fresnel transform domain	2014	[260]
Micromachines	In optical micro-resonators, achieves high-fidelity harmonic production	Algorithm Broyden Fletcher Goldfarb Shanno	High-fidelity harmonic	2020	[261]
APL Photonics	A unique method for eliminating Cross-Phase Modulation (XPM) coherent artifacts in ultrafast pumping	XPMnet algorithm	Cross-phase modulation	2021	[262]
IEEE Photonics Journal	Showcases an optical phase conjugation photoelectric nonlinear compensation method	Complex-valued deep NN	Optical phase conjugation	2021	[263]
Optics Express	The deep residual network is used to forecast the Raman spectra of ice and water to detect the ice-water contact as an identification challenge	Deep-learning-based component identification for mixed Raman spectra	Raman scattering	2019	[264]
Environmental Science and Pollution Research	Examines the impact of the fungicide difenoconazole on the quality of rat sperm	Compare the effectiveness of three categorization algorithms	Raman scattering	2019	[265]
IEICE Communications Express	Improved performance in terms of bit error rate and error vector magnitude by effectively compensating for the nonlinear distortion brought on by cross-phase modulation	A cutting-edge digital signal processing method based on ANN for cross-phase modulation correction	Cross-phase modulation	2018	[266]
Optics Communications	Creates empirical physical formulations based on experimental evidence for the light-scattering amplitude response functions of nematic liquid crystals, which are intrinsically nonlinear	Layered feedforward ANN	Light-scattering	2011	[267]
IEICE Communications Express	Compensates nonlinear distortion in optical communication systems	A three-layer ANN	Self-phase modulation	2017	[268]
Scientific Reports	SHG coefficients of NLO crystals with different diamond-like features are being studied	Random forests regression	Second-harmonic generation	2020	[269]
IEEE Journal of Selected Topics in Quantum Electronics	A nonlinear activation function in a feed forward optical NN	Optical ANN	Electro-optic	2019	[270]

Table 4. *Cont.*

| Journal	Application	Algorithm	Nonlinear Optical	Year	Reference
2019 9th International Conference on Cloud Computing	Provides scenarios that demonstrate the relationship between quantum computers and a light of light in the NLO	Algorithm assisting photonic operations	Four-wave mixing and cross-phase	2019	[271]
Chemical Communications	Ratiometric analysis is used to provide a model for the prediction of the depth of two "flavors" of SERS active nanotags buried inside pig tissue	A proof-of-concept approach for the prediction	Raman scattering	2022	[272]
International Journal of Optics	Inference abilities for the task of classifying images	The deep NN with all-optical diffraction	Nonlinear diffraction	2021	[273]
Advanced Photonics	Enhancement of the third-harmonic generation in optimized metasurfaces and contributes to improving the amplitude of optomechanical vibrations	Deep learning techniques for the inverse design of nanophotonics	Third-harmonic generation	2020	[274]
Conference on Lasers and Electro-Optics	Performs image and audio classification	A universal algorithm for backpropagating	Second-harmonic generation	2021	[275]
Optical Materials Express	Activation functions for fully connected ANN, emulated in tensor flow	Photonic ANN	Induced transparency and reverse saturated absorption	2018	[276]
Optik	Encryption security has been improved to the greatest extent possible to fend off attempts	Modified Gerchberg Saxton Iterative Algorithm	Optical nonlinear cryptosystem	2021	[277]
Optics and Lasers in Engineering	Checks the security of a dual random-phase-coding-based nonlinear optical cryptosystem	chosen-plaintext attack algorithm and known-plaintext attack algorithm modifications	Based on double random phase encoding, the NLO cryptosystem	2021	[278]
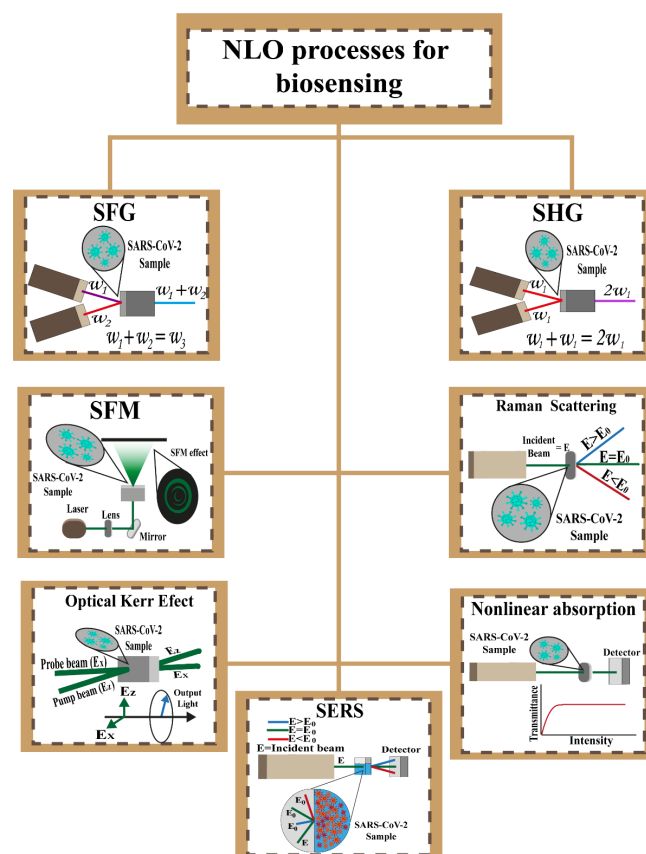
Figure 5. NLO effect schemes proposed for biosensing.

5. Perspectives

Optical biosensors have evolved to visualize biological functions as a microscope has evolved to identify effects of energy. Some optical biosensors can focus the impact of optical and multiphoton nonlinearities to detect the SARS-CoV-2 virus. The optical effect of fluorescence has been used to identify the SARS-CoV-2 virus as well as bacteria, cancer cells, and other viruses. The signature of optics in biosensors has taken advantage of the collection of more information for the detection of biological agents as a non-invasive tool.

Due to the frequency and phase-changing capabilities of the laser light that interacts with NLO materials, they rank among the most intelligent materials of our time [264]. A cutting-edge topic of study for the theoretical and experimental community is the creation of NLO documents [279]. Organic materials must have relatively nonlinear properties due to electrons moving to orbits $\pi - \pi$ [280]. This expectation explains the extensive research on NLO materials for developing biocrystals.

The use of organic crystals as NLO materials has been increasingly promoted by the easy manipulation of these crystals, allowing control of the NLO properties of the material. Compounds exhibiting strong nonlinearity are of great interest to the field of nonlinear optics, as they are used to fabricate devices operating at high speeds [281]. Researchers have been able to produce silicon-organic hybrid waveguides with bandwidths as high as 100 Gbit per second using organic NLO materials [282].

Optical biosensors can be applied to acquire information from remote sensing and one of the tools used for the interpretation of information can be based on ML. The function of the use of ML in biosensors allows automating the device to perform an action depending on the information collected. The diverse forms of emission and optical absorption in nonlinear biosensors are fascinating and are unexplored in several conditions that can be addressed by ML techniques for describing biological functions.

The disadvantage of AI derivatives is that there is a paucity of existing information on studies with NLO effects and nanomaterials, but this opens up an opportunity for new discoveries.

In the collection of information, different algorithms were found that analyze NLO effects. In Table 4, some algorithms are observed in different applications; NLO processes are unexplored for designing platforms related to biosensing performance, but they have promising potential.

6. Conclusions

ML has the potential to fundamentally change the practice of data analysis. Optical biosensors are well positioned to take advantage of ML, which leads to greater efficiency and precision. By combining the ML analysis tools and multiphotonic effects for the increase in applications in optical biosensors, it is clear that there is potential for a better interpretation of biological agents. In this work, a perspective for optical biosensors in virus detection is described.

The processing and classification of large amounts of data allowed by ML lead to extraordinary interpretations and unique predictions in the study with optical biosensors. In this work, optical biosensors assisted by ML for virus detection are proposed, specifically for SARS-CoV-2. By applying different NLO phenomena, the use of ML can optimize the biosensing performance due to its ability to handle large amounts of information. It was pointed out that there is still a vast field of research regarding the party effect of ML on nonlinear optical biosensors.

In this work, it is observed that ML can be useful for estimating different NLO interactions, although the current limited evidence does not support the superiority of ML and automation over study analysis in NLO processes. However, the handling and classification of large amounts of data allow envisioning that ML can play a crucial role in predictions of NLO-based biosensors. In this work, various studies that can be envisioned for the classification and organization of information in experiments with AI are proposed.

References

1. Lei, Z.-L.; Guo, B. 2D Material-Based Optical Biosensor: Status and Prospect. *Adv. Sci.* **2022**, *9*, 2102924. [CrossRef] [PubMed]
2. Khalil, I.; Julkapli, N.; Yehye, W.; Basirun, W.; Bhargava, S. Graphene–Gold Nanoparticles Hybrid—Synthesis, Functionalization, and Application in a Electrochemical and Surface-Enhanced Raman Scattering Biosensor. *Materials* **2016**, *9*, 406. [CrossRef] [PubMed]
3. Malhotra, B.D.; Ali, M.A. Nanomaterials in Biosensors. In *Nanomaterials for Biosensors*; Elsevier: Amsterdam, The Netherlands, 2018; pp. 1–74.
4. Shumeiko, V.; Malach, E.; Helman, Y.; Paltiel, Y.; Bisker, G.; Hayouka, Z.; Shoseyov, O. A Nanoscale Optical Biosensor Based on Peptide Encapsulated SWCNTs for Detection of Acetic Acid in the Gaseous Phase. *Sens. Actuators B Chem.* **2021**, *327*, 128832. [CrossRef]
5. Samani, S.S.; Khojastehnezhad, A.; Ramezani, M.; Alibolandi, M.; Yazdi, F.T.; Mortazavi, S.A.; Khoshbin, Z.; Abnous, K.; Taghdisi, S.M. Ultrasensitive Detection of Micrococcal Nuclease Activity and Staphylococcus Aureus Contamination Using Optical Biosensor Technology-A Review. *Talanta* **2021**, *226*, 122168. [CrossRef]
6. Portes, A.V.R.; Martins, A.J.L.; Guerrero, J.A.; Carvalho, M.M.; Amaya-Fernandez, F.O.; Saito, L.A.M.; Ramirez, J.C. Electro-Optical Biosensor Based on Embedded Double-Monolayer of Graphene Capacitor in Polymer Technology. *Polymers* **2021**, *13*, 3564. [CrossRef]
7. Aldaya, I.; Gil-Molina, A.; Pita, J.L.; Gabrielli, L.H.; Fragnito, H.L.; Dainese, P. Nonlinear Carrier Dynamics in Silicon Nano-Waveguides. *Optica* **2017**, *4*, 1219. [CrossRef]
8. Ramirez, J.C.; Lechuga, L.M.; Gabrielli, L.H.; Hernandez-Figueroa, H.E. Study of a Low-Cost Trimodal Polymer Waveguide for Interferometric Optical Biosensors. *Opt. Express* **2015**, *23*, 11985. [CrossRef]
9. Singh, P. Surface Plasmon Resonance: A Boon for Viral Diagnostics. In *Reference Module in Life Sciences*; Elsevier: Amsterdam, The Netherlands, 2017; ISBN 978-0-12-809633-8.
10. Su, Y.; Xia, S.; Wang, R.; Xiao, L. Phytohormonal Quantification Based on Biological Principles. In *Hormone Metabolism and Signaling in Plants*; Li, J., Li, C., Smith, S.M., Eds.; Elsevier: Amsterdam, The Netherlands, 2017; pp. 431–470. ISBN 978-0-12-811562-6.
11. Cajigas, S.; Soto, D.; Orozco, J. Biosensors: Biosensors With Signal Amplification. In *Reference Module in Biomedical Sciences*; Elsevier: Amsterdam, The Netherlands, 2021; ISBN 978-0-12-801238-3.
12. Shrivastav, A.M.; Cvelbar, U.; Abdulhalim, I. A Comprehensive Review on Plasmonic-Based Biosensors Used in Viral Diagnostics. *Commun. Biol.* **2021**, *4*, 70. [CrossRef] [PubMed]
13. Li, D.; Zhou, H.; Hui, X.; He, X.; Mu, X. Plasmonic Biosensor Augmented by a Genetic Algorithm for Ultra-Rapid, Label-Free, and Multi-Functional Detection of COVID-19. *Anal. Chem.* **2021**, *93*, 9437–9444. [CrossRef]
14. Sharma, S.; Kumar, A. Design of a Biosensor for the Detection of Dengue Virus Using 1D Photonic Crystals. *Plasmonics* **2022**, *17*, 675–680. [CrossRef]
15. Sharma, S.; Kumar, A.; Singh, K.S.; Tyagi, H.K. 2D Photonic Crystal Based Biosensor for the Detection of Chikungunya Virus. *Optik* **2021**, *237*, 166575. [CrossRef]
16. Zhou, J.; Yang, T.; Chen, J.; Wang, C.; Zhang, H.; Shao, Y. Two-Dimensional Nanomaterial-Based Plasmonic Sensing Applications: Advances and Challenges. *Coord. Chem. Rev.* **2020**, *410*, 213218. [CrossRef]
17. Meradi, K.A.; Tayeboun, F.; Guerinik, A.; Zaky, Z.A.; Aly, A.H. Optical Biosensor Based on Enhanced Surface Plasmon Resonance: Theoretical Optimization. *Opt. Quantum Electron.* **2022**, *54*, 124. [CrossRef]
18. Lertvachirapaiboon, C.; Baba, A.; Ekgasit, S.; Shinbo, K.; Kato, K.; Kaneko, F. Transmission Surface Plasmon Resonance Techniques and Their Potential Biosensor Applications. *Biosens. Bioelectron.* **2018**, *99*, 399–415. [CrossRef]

19. Kushwaha, A.S.; Kumar, A.; Kumar, R.; Srivastava, S.K. A Study of Surface Plasmon Resonance (SPR) Based Biosensor with Improved Sensitivity. *Photonics Nanostruct.-Fundam. Appl.* **2018**, *31*, 99–106. [CrossRef]

20. Lu, Y.; Tan, Y.; Xiao, Y.; Li, Z.; Sheng, E.; Dai, Z. A Silver@gold Nanoparticle Tetrahedron Biosensor for Multiple Pesticides Detection Based on Surface-Enhanced Raman Scattering. *Talanta* **2021**, *234*, 122585. [CrossRef] [PubMed]

21. Calvo-Lozano, O.; Sierra, M.; Soler, M.; Estévez, M.C.; Chiscano-Camón, L.; Ruiz-Sanmartin, A.; Ruiz-Rodriguez, J.C.; Ferrer, R.; González-López, J.J.; Esperalba, J.; et al. Label-Free Plasmonic Biosensor for Rapid, Quantitative, and Highly Sensitive COVID-19 Serology: Implementation and Clinical Validation. *Anal. Chem.* **2022**, *94*, 975–984. [CrossRef]

22. Sidhu, R.; Zheng, R.; Rasheed, A.; Khan, M.A. The Development of Point-of-Care Plasmonic-Based Biosensor for Early Detection of COVID-19 Virus. In Proceedings of the 2021 IEEE 15th International Conference on Nano/Molecular Medicine & Engineering (NANOMED), Taipei, Taiwan, 15–17 November 2021; IEEE: Manhattan, NY, USA, 2021; pp. 23–27.

23. Wang, J.; Yao, Z.; Lei, T.; Poon, A.W. Silicon Coupled-Resonator Optical-Waveguide-Based Biosensors Using Light-Scattering Pattern Recognition with Pixelized Mode-Field-Intensity Distributions. *Sci. Rep.* **2015**, *4*, 7528. [CrossRef]

24. Wang, J.; Yao, Z.; Poon, A.W. Silicon-Nitride-Based Integrated Optofluidic Biochemical Sensors Using a Coupled-Resonator Optical Waveguide. *Front. Mater.* **2015**, *2*, 34. [CrossRef]

25. Zhang, P.; Ma, G.; Dong, W.; Wan, Z.; Wang, S.; Tao, N. Plasmonic Scattering Imaging of Single Proteins and Binding Kinetics. *Nat. Methods* **2020**, *17*, 1010–1017. [CrossRef]

26. Song, M.K.; Chen, S.X.; Hu, P.P.; Huang, C.Z.; Zhou, J. Automated Plasmonic Resonance Scattering Imaging Analysis via Deep Learning. *Anal. Chem.* **2021**, *93*, 2619–2626. [CrossRef] [PubMed]

27. Pang, Y.; Wan, N.; Shi, L.; Wang, C.; Sun, Z.; Xiao, R.; Wang, S. Dual-Recognition Surface-Enhanced Raman Scattering(SERS)Biosensor for Pathogenic Bacteria Detection by Using Vancomycin-SERS Tags and Aptamer-Fe_3O_4@Au. *Anal. Chim. Acta* **2019**, *1077*, 288–296. [CrossRef] [PubMed]

28. Mao, K.; Zhou, Z.; Han, S.; Zhou, X.; Hu, J.; Li, X.; Yang, Z. A Novel Biosensor Based on Au@Ag Core-Shell Nanoparticles for Sensitive Detection of Methylamphetamine with Surface Enhanced Raman Scattering. *Talanta* **2018**, *190*, 263–268. [CrossRef] [PubMed]

29. He, X.; Zhou, X.; Liu, Y.; Wang, X. Ultrasensitive, Recyclable and Portable Microfluidic Surface-Enhanced Raman Scattering (SERS) Biosensor for Uranyl Ions Detection. *Sens. Actuators B Chem.* **2020**, *311*, 127676. [CrossRef]

30. Khalil, I.; Yehye, W.A.; Muhd Julkapli, N.; Ibn Sina, A.A.; Islam Chowdhury, F.; Khandaker, M.U.; Hsiao, V.K.S.; Basirun, W.J. Simultaneous Detection of Dual Food Adulterants Using Graphene Oxide and Gold Nanoparticle Based Surface Enhanced Raman Scattering Duplex DNA Biosensor. *Vib. Spectrosc.* **2021**, *116*, 103293. [CrossRef]

31. Vendrell, M.; Maiti, K.K.; Dhaliwal, K.; Chang, Y.-T. Surface-Enhanced Raman Scattering in Cancer Detection and Imaging. *Trends Biotechnol.* **2013**, *31*, 249–257. [CrossRef]

32. Dey, S.; Ahmed, E.; Somvanshi, P.S.; Sina, A.A.I.; Wuethrich, A.; Trau, M. An Electrochemical and Raman Scattering Dual Detection Biosensor for Rapid Screening and Biomolecular Profiling of Cancer Biomarkers. *Chemosensors* **2022**, *10*, 93. [CrossRef]

33. Granger, J.H.; Granger, M.C.; Firpo, M.A.; Mulvihill, S.J.; Porter, M.D. Toward Development of a Surface-Enhanced Raman Scattering (SERS)-Based Cancer Diagnostic Immunoassay Panel. *Analyst* **2013**, *138*, 410–416. [CrossRef]

34. Lopatynskyi, A.M.; Lopatynska, O.G.; Guo, L.J.; Chegel, V.I. Localized Surface Plasmon Resonance Biosensor—Part I: Theoretical Study of Sensitivity—Extended Mie Approach. *IEEE Sens. J.* **2011**, *11*, 361–369. [CrossRef]

35. Manikandan, M.; Revathi, C.; Senthilkumar, P.; Amreetha, S.; Dhanuskodi, S.; Rajendra Kumar, R.T. CdTe Nanorods for Nonenzymatic Hydrogen Peroxide Biosensor and Optical Limiting Applications. *Ionics* **2020**, *26*, 2003–2010. [CrossRef]

36. Prasanna Kumaar, S.; Sivasubramanian, A. Optimization of the Transverse Electric Photonic Strip Waveguide Biosensor for Detecting Diabetes Mellitus from Bulk Sensitivity. *J. Healthc. Eng.* **2021**, *2021*, 6081570. [CrossRef]

37. Panda, A.; Puspa Devi, P. Photonic Crystal Biosensor for Refractive Index Based Cancerous Cell Detection. *Opt. Fiber Technol.* **2020**, *54*, 102123. [CrossRef]

38. Efimov, I.M.; Vanyushkin, N.A.; Gevorgyan, A.H.; Golik, S.S. Optical Biosensor Based on a Photonic Crystal with a Defective Layer Designed to Determine the Concentration of SARS-CoV-2 in Water. *Phys. Scr.* **2022**, *97*, 055506. [CrossRef]

39. Abrego-Martinez, J.C.; Jafari, M.; Chergui, S.; Pavel, C.; Che, D.; Siaj, M. Aptamer-Based Electrochemical Biosensor for Rapid Detection of SARS-CoV-2: Nanoscale Electrode-Aptamer-SARS-CoV-2 Imaging by Photo-Induced Force Microscopy. *Biosens. Bioelectron.* **2022**, *195*, 113595. [CrossRef]

40. Ranjan, A.K.; Patra, A.K.; Gorai, A.K. Effect of Lockdown Due to SARS COVID-19 on Aerosol Optical Depth (AOD) over Urban and Mining Regions in India. *Sci. Total Environ.* **2020**, *745*, 141024. [CrossRef]

41. Cennamo, N.; D'Agostino, G.; Perri, C.; Arcadio, F.; Chiaretti, G.; Parisio, E.M.; Camarlinghi, G.; Vettori, C.; Di Marzo, F.; Cennamo, R.; et al. Proof of Concept for a Quick and Highly Sensitive On-Site Detection of SARS-CoV-2 by Plasmonic Optical Fibers and Molecularly Imprinted Polymers. *Sensors* **2021**, *21*, 1681. [CrossRef]

42. Liu, Y.-N.; Lv, Z.-T.; Yang, S.-Y.; Liu, X.-W. Optical Tracking of the Interfacial Dynamics of Single SARS-CoV-2 Pseudoviruses. *Environ. Sci. Technol.* **2021**, *55*, 4115–4122. [CrossRef]

43. Gomez-Gonzalez, E.; Barriga-Rivera, A.; Fernandez-Muñoz, B.; Navas-Garcia, J.M.; Fernandez-Lizaranzu, I.; Munoz-Gonzalez, F.J.; Parrilla-Giraldez, R.; Requena-Lancharro, D.; Gil-Gamboa, P.; Rosell-Valle, C.; et al. Optical Imaging Spectroscopy for Rapid, Primary Screening of SARS-CoV-2: A Proof of Concept. *Sci. Rep.* **2022**, *12*, 2356. [CrossRef]

44. Daoudi, K.; Ramachandran, K.; Alawadhi, H.; Boukherroub, R.; Dogheche, E.; El Khakani, M.A.; Gaidi, M. Ultra-Sensitive and Fast Optical Detection of the Spike Protein of the SARS-CoV-2 Using AgNPs/SiNWs Nanohybrid Based Sensors. *Surf. Interfaces* **2021**, *27*, 101454. [CrossRef]

45. Li, Z.; Hirst, J.D. Computed Optical Spectra of SARS-CoV-2 Proteins. *Chem. Phys. Lett.* **2020**, *758*, 137935. [CrossRef]

46. Rabiee, N.; Fatahi, Y.; Ahmadi, S.; Abbariki, N.; Ojaghi, A.; Rabiee, M.; Radmanesh, F.; Dinarvand, R.; Bagherzadeh, M.; Mostafavi, E.; et al. Bioactive Hybrid Metal-Organic Framework (MOF)-Based Nanosensors for Optical Detection of Recombinant SARS-CoV-2 Spike Antigen. *Sci. Total Environ.* **2022**, *825*, 153902. [CrossRef] [PubMed]

47. Minopoli, A.; Scardapane, E.; Acunzo, A.; Campanile, R.; Della Ventura, B.; Velotta, R. Analysis of the Optical Response of a SARS-CoV-2-Directed Colorimetric Immunosensor. *AIP Adv.* **2021**, *11*, 065319. [CrossRef]

48. Diaz, L.M.; Johnson, B.E.; Jenkins, D.M. Real-Time Optical Analysis of a Colorimetric LAMP Assay for SARS-CoV-2 in Saliva with a Handheld Instrument Improves Accuracy Compared with Endpoint Assessment. *J. Biomol. Tech.* **2021**, *32*, 158–171. [CrossRef] [PubMed]

49. Tao, Y.; Bian, S.; Wang, P.; Zhang, H.; Bi, W.; Zhu, P.; Sawan, M. Rapid Optical Biosensing of SARS-CoV-2 Spike Proteins in Artificial Samples. *Sensors* **2022**, *22*, 3768. [CrossRef]

50. Xu, W.; Liu, J.; Song, D.; Li, C.; Zhu, A.; Long, F. Rapid, Label-Free, and Sensitive Point-of-Care Testing of Anti-SARS-CoV-2 IgM/IgG Using All-Fiber Fresnel Reflection Microfluidic Biosensor. *Microchim. Acta* **2021**, *188*, 261. [CrossRef]

51. Doulou, S.; Leventogiannis, K.; Tsilika, M.; Rodencal, M.; Katrini, K.; Antonakos, N.; Kyprianou, M.; Karofylakis, E.; Karageorgos, A.; Koufargyris, P.; et al. A Novel Optical Biosensor for the Early Diagnosis of Sepsis and Severe Covid-19: The PROUD Study. *BMC Infect. Dis.* **2020**, *20*, 860. [CrossRef]

52. Courtney, S.; Stromberg, Z.; Myers y Gutiérrez, A.; Jacobsen, D.; Stromberg, L.; Lenz, K.; Theiler, J.; Foley, B.; Gans, J.; Yusim, K.; et al. Optical Biosensor Platforms Display Varying Sensitivity for the Direct Detection of Influenza RNA. *Biosensors* **2021**, *11*, 367. [CrossRef]

53. Schotter, J.; Schrittwieser, S.; Muellner, P.; Melnik, E.; Hainberger, R.; Koppitsch, G.; Schrank, F.; Soulantika, K.; Lentijo-Mozo, S.; Pelaz, B.; et al. Optical Biosensor Technologies for Molecular Diagnostics at the Point-of-Care. *Proc. SPIE* **2015**, *9490*, 94900B. [CrossRef]

54. El-Sherif, D.M.; Abouzid, M.; Gaballah, M.S.; Ahmed, A.A.; Adeel, M.; Sheta, S.M. New Approach in SARS-CoV-2 Surveillance Using Biosensor Technology: A Review. *Environ. Sci. Pollut. Res.* **2022**, *29*, 1677–1695. [CrossRef]

55. Lee, S.-L.; Kim, J.; Choi, S.; Han, J.; Seo, G.; Lee, Y.W. Fiber-Optic Label-Free Biosensor for SARS-CoV-2 Spike Protein Detection Using Biofunctionalized Long-Period Fiber Grating. *Talanta* **2021**, *235*, 122801. [CrossRef]

56. Sun, Y.; Shi, L.; Mi, L.; Guo, R.; Li, T. Recent Progress of SERS Optical Nanosensors for MiRNA Analysis. *J. Mater. Chem. B* **2020**, *8*, 5178–5183. [CrossRef] [PubMed]

57. Yildirim, D.U.; Ghobadi, A.; Ozbay, E. Nanosensors Based on Localized Surface Plasmon Resonance. In *Plasmonic Sensors and Their Applications*; Wiley Online Books; Wiley: Hoboken, NJ, USA, 2021; pp. 23–54, ISBN 9783527830343.

58. Dziekan, Z.; Pituła, E.; Kwietniewski, N.; Stonio, B.; Janik, M.; Śmiarowski, T.; Koba, M.; Parzuchowski, P.; Niedziółka-Jönsson, J.; Śmietana, M. Performance of Nanoimprinted and Nanocoated Optical Label-Free Biosensor-Nanocoating Properties Perspective. *Opt. Lasers Eng.* **2022**, *153*, 107009. [CrossRef]

59. Threm, D.; Nazirizadeh, Y.; Gerken, M. Photonic Crystal Biosensors towards On-Chip Integration. *J. Biophotonics* **2012**, *5*, 601–616. [CrossRef]

60. Fernández Gavela, A.; Grajales García, D.; Ramirez, J.; Lechuga, L. Last Advances in Silicon-Based Optical Biosensors. *Sensors* **2016**, *16*, 285. [CrossRef] [PubMed]

61. Srivastava, A.; Sharma, A.K.; Kumar Prajapati, Y. On the Sensitivity-Enhancement in Plasmonic Biosensor with Photonic Spin Hall Effect at Visible Wavelength. *Chem. Phys. Lett.* **2021**, *774*, 138613. [CrossRef]

62. Li, N.; Tang, T.; Li, J.; Luo, L.; Li, C.; Shen, J.; Yao, J. Highly Sensitive Biosensor with Graphene-MoS$_2$ Heterostructure Based on Photonic Spin Hall Effect. *J. Magn. Magn. Mater.* **2019**, *484*, 445–450. [CrossRef]

63. Leuermann, J.; Stamenkovic, V.; Ramirez-Priego, P.; Sánchez-Postigo, A.; Fernández-Gavela, A.; Chapman, C.A.; Bailey, R.C.; Lechuga, L.M.; Perez-Inestrosa, E.; Collado, D.; et al. Coherent Silicon Photonic Interferometric Biosensor with an Inexpensive Laser Source for Sensitive Label-Free Immunoassays. *Opt. Lett.* **2020**, *45*, 6595. [CrossRef]

64. Xie, L.; Zhang, Z.; Du, J. The Photonic Spin Hall Effect Sensor. In *Applied Optical Metrology II*; Novak, E., Trolinger, J.D., Eds.; SPIE: Bellingham, WA, USA, 2017; Volume 10373, p. 10.

65. Mavrikou, S.; Moschopoulou, G.; Tsekouras, V.; Kintzios, S. Development of a Portable, Ultra-Rapid and Ultra-Sensitive Cell-Based Biosensor for the Direct Detection of the SARS-CoV-2 S1 Spike Protein Antigen. *Sensors* **2020**, *20*, 3121. [CrossRef]

66. Wrapp, D.; Wang, N.; Corbett, K.S.; Goldsmith, J.A.; Hsieh, C.-L.; Abiona, O.; Graham, B.S.; McLellan, J.S. Cryo-EM Structure of the 2019-NCoV Spike in the Prefusion Conformation. *Science* **2020**, *367*, 1260–1263. [CrossRef]

67. Ruiz-Vega, G.; Soler, M.; Lechuga, L.M. Nanophotonic Biosensors for Point-of-Care COVID-19 Diagnostics and Coronavirus Surveillance. *J. Phys. Photonics* **2021**, *3*, 011002. [CrossRef]

68. Moznuzzaman, M.; Khan, I.; Islam, M.R. Nano-Layered Surface Plasmon Resonance-Based Highly Sensitive Biosensor for Virus Detection: A Theoretical Approach to Detect SARS-CoV-2. *AIP Adv.* **2021**, *11*, 065023. [CrossRef] [PubMed]

69. Bai, H.; Wang, R.; Hargis, B.; Lu, H.; Li, Y. A SPR Aptasensor for Detection of Avian Influenza Virus H5N1. *Sensors* **2012**, *12*, 12506–12518. [CrossRef] [PubMed]

70. Prabowo, B.A.; Wang, R.Y.L.; Secario, M.K.; Ou, P.-T.; Alom, A.; Liu, J.-J.; Liu, K.-C. Rapid Detection and Quantification of Enterovirus 71 by a Portable Surface Plasmon Resonance Biosensor. *Biosens. Bioelectron.* **2017**, *92*, 186–191. [CrossRef]

71. Murugan, D.; Bhatia, H.; Sai, V.V.R.; Satija, J. P-FAB: A Fiber-Optic Biosensor Device for Rapid Detection of COVID-19. *Trans. Indian Natl. Acad. Eng.* **2020**, *5*, 211–215. [CrossRef]

72. Alathari, M.J.A.; Al Mashhadany, Y.; Mokhtar, M.H.H.; Burham, N.; Bin Zan, M.S.D.; A Bakar, A.A.; Arsad, N. Human Body Performance with COVID-19 Affectation According to Virus Specification Based on Biosensor Techniques. *Sensors* **2021**, *21*, 8362. [CrossRef]

73. Taha, B.A.; Al Mashhadany, Y.; Hafiz Mokhtar, M.H.; Dzulkefly Bin Zan, M.S.; Arsad, N. An Analysis Review of Detection Coronavirus Disease 2019 (COVID-19) Based on Biosensor Application. *Sensors* **2020**, *20*, 6764. [CrossRef] [PubMed]

74. Ma, R.-M.; Oulton, R.F. Applications of Nanolasers. *Nat. Nanotechnol.* **2019**, *14*, 12–22. [CrossRef]

75. Rodriguez, G.A.; Markov, P.; Cartwright, A.P.; Choudhury, M.H.; Afzal, F.O.; Cao, T.; Halimi, S.I.; Retterer, S.T.; Kravchenko, I.I.; Weiss, S.M. Photonic Crystal Nanobeam Biosensors Based on Porous Silicon. *Opt. Express* **2019**, *27*, 9536. [CrossRef]

76. Kim, H.; Hwang, J.; Kim, J.H.; Lee, S.; Kang, M. Sensitive Detection of Multiple Fluoresence Probes Based on Surface-Enhanced Raman Scattering (SERS) for MERS-CoV. In Proceedings of the 2019 IEEE 14th International Conference on Nano/Micro Engineered and Molecular Systems (NEMS), Bangkok, Thailand, 11–14 April 2019; IEEE: Manhattan, NY, USA, 2019; pp. 498–501.

77. Kumar, A.; Kumar, A.; Kushwaha, A.S.; Dubey, S.K.; Srivastava, S.K. A Comparative Study of Different Types of Sandwiched Structures of SPR Biosensor for Sensitive Detection of SsDNA. *Photonics Nanostruct.-Fundam. Appl.* **2022**, *48*, 100984. [CrossRef]

78. Syed Nor, S.N.; Rasanang, N.S.; Karman, S.; Zaman, W.S.W.K.; Harun, S.W.; Arof, H. A Review: Surface Plasmon Resonance-Based Biosensor for Early Screening of SARS-CoV2 Infection. *IEEE Access* **2022**, *10*, 1228–1244. [CrossRef]

79. Yang, Y.; Liu, J.; Zhou, X. A CRISPR-Based and Post-Amplification Coupled SARS-CoV-2 Detection with a Portable Evanescent Wave Biosensor. *Biosens. Bioelectron.* **2021**, *190*, 113418. [CrossRef] [PubMed]

80. Cavalera, S.; Colitti, B.; Rosati, S.; Ferrara, G.; Bertolotti, L.; Nogarol, C.; Guiotto, C.; Cagnazzo, C.; Denina, M.; Fagioli, F.; et al. A Multi-Target Lateral Flow Immunoassay Enabling the Specific and Sensitive Detection of Total Antibodies to SARS CoV-2. *Talanta* **2021**, *223*, 121737. [CrossRef] [PubMed]

81. Song, D.; Liu, J.; Xu, W.; Han, X.; Wang, H.; Cheng, Y.; Zhuo, Y.; Long, F. Rapid and Quantitative Detection of SARS-CoV-2 IgG Antibody in Serum Using Optofluidic Point-of-Care Testing Fluorescence Biosensor. *Talanta* **2021**, *235*, 122800. [CrossRef]

82. Han, H.; Wang, C.; Yang, X.; Zheng, S.; Cheng, X.; Liu, Z.; Zhao, B.; Xiao, R. Rapid Field Determination of SARS-CoV-2 by a Colorimetric and Fluorescent Dual-Functional Lateral Flow Immunoassay Biosensor. *Sens. Actuators B Chem.* **2022**, *351*, 130897. [CrossRef]

83. Zhang, K.; Fan, Z.; Ding, Y.; Xie, M. A PH-Engineering Regenerative DNA Tetrahedron ECL Biosensor for the Assay of SARS-CoV-2 RdRp Gene Based on CRISPR/Cas12a Trans-Activity. *Chem. Eng. J.* **2022**, *429*, 132472. [CrossRef]

84. Zhang, K.; Fan, Z.; Ding, Y.; Zhu, S.; Xie, M.; Hao, N. Exploring the Entropy-Driven Amplification Reaction and Trans -Cleavage Activity of CRISPR-Cas12a for the Development of an Electrochemiluminescence Biosensor for the Detection of the SARS-CoV-2 RdRp Gene in Real Samples and Environmental Surveillance. *Environ. Sci. Nano* **2022**, *9*, 162–172. [CrossRef]

85. Xi, H.; Juhas, M.; Zhang, Y. G-Quadruplex Based Biosensor: A Potential Tool for SARS-CoV-2 Detection. *Biosens. Bioelectron.* **2020**, *167*, 112494. [CrossRef]

86. O'Brien, A.; Chen, D.-Y.; Hackbart, M.; Close, B.J.; O'Brien, T.E.; Saeed, M.; Baker, S.C. Detecting SARS-CoV-2 3CLpro Expression and Activity Using a Polyclonal Antiserum and a Luciferase-Based Biosensor. *Virology* **2021**, *556*, 73–78. [CrossRef]

87. Zhang, K.; Fan, Z.; Huang, Y.; Ding, Y.; Xie, M.; Wang, M. Hybridization Chain Reaction Circuit-Based Electrochemiluminescent Biosensor for SARS-Cov-2 RdRp Gene Assay. *Talanta* **2022**, *240*, 123207. [CrossRef] [PubMed]

88. Fan, Z.; Yao, B.; Ding, Y.; Xu, D.; Zhao, J.; Zhang, K. Rational Engineering the DNA Tetrahedrons of Dual Wavelength Ratiometric Electrochemiluminescence Biosensor for High Efficient Detection of SARS-CoV-2 RdRp Gene by Using Entropy-Driven and Bipedal DNA Walker Amplification Strategy. *Chem. Eng. J.* **2022**, *427*, 131686. [CrossRef]

89. Yang, X.; Liu, L.; Hao, Y.; So, E.; Emami, S.S.; Zhang, D.; Gong, Y.; Sheth, P.M.; Wang, Y. A Bioluminescent Biosensor for Quantifying the Interaction of SARS-CoV-2 and Its Receptor ACE2 in Cells and In Vitro. *Viruses* **2021**, *13*, 1055. [CrossRef] [PubMed]

90. Yang, X.; Liu, L.; Hao, Y.; So, Y.W.; Emami, S.S.; Zhang, D.; Gong, Y.; Sheth, P.M.; Wang, Y.T. An Ultrasensitive Biosensor for Quantifying the Interaction of SARS-CoV-2 and Its Receptor ACE2 in Cells and In Vitro. *bioRxiv* **2020**, 424698. [CrossRef]

91. Murillo, A.M.M.; Tomé-Amat, J.; Ramírez, Y.; Garrido-Arandia, M.; Valle, L.G.; Hernández-Ramírez, G.; Tramarin, L.; Herreros, P.; Santamaría, B.; Díaz-Perales, A.; et al. Developing an Optical Interferometric Detection Method Based Biosensor for Detecting Specific SARS-CoV-2 Immunoglobulins in Serum and Saliva, and Their Corresponding ELISA Correlation. *Sens. Actuators B Chem.* **2021**, *345*, 130394. [CrossRef]

92. Liu, N.; Wang, S.; Wang, J.; Lv, J.; Cheng, Q.; Ma, W.; Lu, Y. Promising Refractive Index and Temperature Biosensor Based on Hybrid Gmr/Fp System Employed for the Detection of SARS-CoV-2. *SSRN Electron. J.* **2022**. [CrossRef]

93. Gutiérrez-Gálvez, L.; del Caño, R.; Menéndez-Luque, I.; García-Nieto, D.; Rodríguez-Peña, M.; Luna, M.; Pineda, T.; Pariente, F.; García-Mendiola, T.; Lorenzo, E. Electrochemiluminescent Nanostructured DNA Biosensor for SARS-CoV-2 Detection. *Talanta* **2022**, *240*, 123203. [CrossRef] [PubMed]

94. Jiang, C.; Mu, X.; Liu, S.; Liu, Z.; Du, B.; Wang, J.; Xu, J. A Study of the Detection of SARS-CoV-2 ORF1ab Gene by the Use of Electrochemiluminescent Biosensor Based on Dual-Probe Hybridization. *Sensors* **2022**, *22*, 2402. [CrossRef]

95. Karakuş, E.; Erdemir, E.; Demirbilek, N.; Liv, L. Colorimetric and Electrochemical Detection of SARS-CoV-2 Spike Antigen with a Gold Nanoparticle-Based Biosensor. *Anal. Chim. Acta* **2021**, *1182*, 338939. [CrossRef]
96. Xu, W.; Zhuo, Y.; Song, D.; Han, X.; Xu, J.; Long, F. Development of a Novel Label-Free All-Fiber Optofluidic Biosensor Based on Fresnel Reflection and Its Applications. *Anal. Chim. Acta* **2021**, *1181*, 338910. [CrossRef] [PubMed]
97. Kim, M. Detecting SARS-CoV-2 with a Rapid, Cost-Effective Colorimetric Biosensor. *Scilight* **2021**, *2021*, 251103. [CrossRef]
98. Sampad, M.J.N.; Zhang, H.; Yuzvinsky, T.D.; Stott, M.A.; Hawkins, A.R.; Schmidt, H. Optical Trapping Assisted Label-Free and Amplification-Free Detection of SARS-CoV-2 RNAs with an Optofluidic Nanopore Sensor. *Biosens. Bioelectron.* **2021**, *194*, 113588. [CrossRef]
99. Ahmad, M.; Sharma, P.; Kamai, A.; Agrawal, A.; Faruq, M.; Kulshreshtha, A. HRPZyme Assisted Recognition of SARS-CoV-2 Infection by Optical Measurement (HARIOM). *Biosens. Bioelectron.* **2021**, *187*, 113280. [CrossRef]
100. Ravalin, M.; Roh, H.; Suryawanshi, R.; Kumar, G.R.; Pak, J.E.; Ott, M.; Ting, A.Y. A Single-Component Luminescent Biosensor for the SARS-CoV-2 Spike Protein. *J. Am. Chem. Soc.* **2022**, *144*, 13663–13672. [CrossRef]
101. Huang, L.; Ding, L.; Zhou, J.; Chen, S.; Chen, F.; Zhao, C.; Xu, J.; Hu, W.; Ji, J.; Xu, H.; et al. One-Step Rapid Quantification of SARS-CoV-2 Virus Particles via Low-Cost Nanoplasmonic Sensors in Generic Microplate Reader and Point-of-Care Device. *Biosens. Bioelectron.* **2021**, *171*, 112685. [CrossRef] [PubMed]
102. Yao, B.; Zhang, J.; Fan, Z.; Ding, Y.; Zhou, B.; Yang, R.; Zhao, J.; Zhang, K. Rational Engineering of the DNA Walker Amplification Strategy by Using a Au@Ti$_3$C$_2$@PEI-Ru(Dcbpy)32+ Nanocomposite Biosensor for Detection of the SARS-CoV-2 RdRp Gene. *ACS Appl. Mater. Interfaces* **2021**, *13*, 19816–19824. [CrossRef]
103. Bhattacharjee, A.; Sabino, R.M.; Gangwish, J.; Manivasagam, V.K.; James, S.; Popat, K.C.; Reynolds, M.; Li, Y.V. A Novel Colorimetric Biosensor for Detecting SARS-CoV-2 by Utilizing the Interaction between Nucleocapsid Antibody and Spike Proteins. *Vitr. Model.* **2022**, *1*, 241–247. [CrossRef]
104. Lee, C.Y.; Degani, I.; Cheong, J.; Lee, J.-H.; Choi, H.-J.; Cheon, J.; Lee, H. Fluorescence Polarization System for Rapid COVID-19 Diagnosis. *Biosens. Bioelectron.* **2021**, *178*, 113049. [CrossRef] [PubMed]
105. Roda, A.; Cavalera, S.; Di Nardo, F.; Calabria, D.; Rosati, S.; Simoni, P.; Colitti, B.; Baggiani, C.; Roda, M.; Anfossi, L. Dual Lateral Flow Optical/Chemiluminescence Immunosensors for the Rapid Detection of Salivary and Serum IgA in Patients with COVID-19 Disease. *Biosens. Bioelectron.* **2021**, *172*, 112765. [CrossRef] [PubMed]
106. Zheng, Y.; Song, K.; Cai, K.; Liu, L.; Tang, D.; Long, W.; Zhai, B.; Chen, J.; Tao, Y.; Zhao, Y.; et al. B-Cell-Epitope-Based Fluorescent Quantum Dot Biosensors for SARS-CoV-2 Enable Highly Sensitive COVID-19 Antibody Detection. *Viruses* **2022**, *14*, 1031. [CrossRef]
107. Büyüksünetçi, Y.T.; Çitil, B.E.; Tapan, U.; Anık, Ü. Development and Application of a SARS-CoV-2 Colorimetric Biosensor Based on the Peroxidase-Mimic Activity of γ-Fe$_2$O$_3$ Nanoparticles. *Microchim. Acta* **2021**, *188*, 335. [CrossRef]
108. Divagar, M.; Gayathri, R.; Rasool, R.; Shamlee, J.K.; Bhatia, H.; Satija, J.; Sai, V.V.R. Plasmonic Fiberoptic Absorbance Biosensor (P-FAB) for Rapid Detection of SARS-CoV-2 Nucleocapsid Protein. *IEEE Sens. J.* **2021**, *21*, 22758–22766. [CrossRef]
109. Zheng, Y.; Bian, S.; Sun, J.; Wen, L.; Rong, G.; Sawan, M. Label-Free LSPR-Vertical Microcavity Biosensor for On-Site SARS-CoV-2 Detection. *Biosensors* **2022**, *12*, 151. [CrossRef] [PubMed]
110. Zhang, M.; Li, X.; Pan, J.; Zhang, Y.; Zhang, L.; Wang, C.; Yan, X.; Liu, X.; Lu, G. Ultrasensitive Detection of SARS-CoV-2 Spike Protein in Untreated Saliva Using SERS-Based Biosensor. *Biosens. Bioelectron.* **2021**, *190*, 113421. [CrossRef] [PubMed]
111. Li, Y.; Lin, C.; Peng, Y.; He, J.; Yang, Y. High-Sensitivity and Point-of-Care Detection of SARS-CoV-2 from Nasal and Throat Swabs by Magnetic SERS Biosensor. *Sens. Actuators B Chem.* **2022**, *365*, 131974. [CrossRef]
112. Hojjat Jodaylami, M.; Djaileb, A.; Live, L.S.; Boudreau, D.; Pelletier, J.; Masson, J.-F. Rapid Quantification of SARS-CoV-2 Antibodies with a Portable Surface Plasmon Resonance Biosensor. *ECS Meet. Abstr.* **2021**, *MA2021-01*, 2026. [CrossRef]
113. Cady, N.C.; Tokranova, N.; Minor, A.; Nikvand, N.; Strle, K.; Lee, W.T.; Page, W.; Guignon, E.; Pilar, A.; Gibson, G.N. Multiplexed Detection and Quantification of Human Antibody Response to COVID-19 Infection Using a Plasmon Enhanced Biosensor Platform. *Biosens. Bioelectron.* **2021**, *171*, 112679. [CrossRef] [PubMed]
114. Cognetti, J.S.; Miller, B.L. Monitoring Serum Spike Protein with Disposable Photonic Biosensors Following SARS-CoV-2 Vaccination. *Sensors* **2021**, *21*, 5857. [CrossRef] [PubMed]
115. Wu, Q.; Wu, W.; Chen, F.; Ren, P. Highly Sensitive and Selective Surface Plasmon Resonance Biosensor for the Detection of SARS-CoV-2 Spike S1 Protein. *Analyst* **2022**, *147*, 2809–2818. [CrossRef]
116. Ebrem Bilgin, B.; Torun, H.; Ilgü, M.; Yanik, C.; Batur, S.N.; Çelik, S.; Öztürk, M.; Dogan, Ö.; Ergönül, Ö.; Solaroglu, I.; et al. Clinical Validation of SERS Metasurface SARS-CoV-2 Biosensor. In *Biomedical Vibrational Spectroscopy 2022: Advances in Research and Industry*; Huang, Z., Ed.; SPIE: Bellingham, WA, USA, 2022; Volume 11957, p. 36.
117. Kumar, A.; Kumar, A.; Srivastava, S.K. Silicon Nitride-BP-Based Surface Plasmon Resonance Highly Sensitive Biosensor for Virus SARS-CoV-2 Detection. *Plasmonics* **2022**, *17*, 1065–1077. [CrossRef]
118. Akib, T.B.A.; Mou, S.F.; Rahman, M.M.; Rana, M.M.; Islam, M.R.; Mehedi, I.M.; Mahmud, M.A.P.; Kouzani, A.Z. Design and Numerical Analysis of a Graphene-Coated SPR Biosensor for Rapid Detection of the Novel Coronavirus. *Sensors* **2021**, *21*, 3491. [CrossRef]
119. Anshori, I.; Nugroho, A.E.; Jessika, A.S.; Yusuf, M.; Hartati, Y.W.; Sari, S.P.; Tohari, T.R.; Yuliarto, B.; Gumilar, G.; Nuraviana, L.; et al. Single-Chained Fragment Variable (ScFv) Recombinant as a Potential Receptor for SARS-CoV-2 Biosensor Based on Surface Plasmon Resonance (SPR). In *2021 IEEE Sensors*; IEEE: Piscataway, NJ, USA, 2021; p. 21487738.

120. Dai, Z.; Xu, X.; Wang, Y.; Li, M.; Zhou, K.; Zhang, L.; Tan, Y. Surface Plasmon Resonance Biosensor with Laser Heterodyne Feedback for Highly-Sensitive and Rapid Detection of COVID-19 Spike Antigen. *Biosens. Bioelectron.* **2022**, *206*, 114163. [CrossRef]
121. Peng, Y.; Lin, C.; Li, Y.; Gao, Y.; Wang, J.; He, J.; Huang, Z.; Liu, J.; Luo, X.; Yang, Y. Identifying Infectiousness of SARS-CoV-2 by Ultra-Sensitive SnS$_2$ SERS Biosensors with Capillary Effect. *Matter* **2022**, *5*, 694–709. [CrossRef] [PubMed]
122. Lee, W.-I.; Subramanian, A.; Mueller, S.; Levon, K.; Nam, C.-Y.; Rafailovich, M.H. Potentiometric Biosensors Based on Molecular-Imprinted Self-Assembled Monolayer Films for Rapid Detection of Influenza A Virus and SARS-CoV-2 Spike Protein. *ACS Appl. Nano Mater.* **2022**, *5*, 5045–5055. [CrossRef] [PubMed]
123. Qiu, G.; Gai, Z.; Tao, Y.; Schmitt, J.; Kullak-Ublick, G.A.; Wang, J. Dual-Functional Plasmonic Photothermal Biosensors for Highly Accurate Severe Acute Respiratory Syndrome Coronavirus 2 Detection. *ACS Nano* **2020**, *14*, 5268–5277. [CrossRef] [PubMed]
124. Forssén, P.; Samuelsson, J.; Lacki, K.; Fornstedt, T. Advanced Analysis of Biosensor Data for SARS-CoV-2 RBD and ACE2 Interactions. *Anal. Chem.* **2020**, *92*, 11520–11524. [CrossRef]
125. Behrouzi, K.; Lin, L. Gold Nanoparticle Based Plasmonic Sensing for the Detection of SARS-CoV-2 Nucleocapsid Proteins. *Biosens. Bioelectron.* **2022**, *195*, 113669. [CrossRef]
126. Basso, C.R.; Malossi, C.D.; Haisi, A.; de Albuquerque Pedrosa, V.; Barbosa, A.N.; Grotto, R.T.; Araujo Junior, J.P. Fast and Reliable Detection of SARS-CoV-2 Antibodies Based on Surface Plasmon Resonance. *Anal. Methods* **2021**, *13*, 3297–3306. [CrossRef]
127. Saada, H.; Pagneux, Q.; Wei, J.; Live, L.; Roussel, A.; Dogliani, A.; Die Morini, L.; Engelmann, I.; Alidjinou, E.K.; Rolland, A.S.; et al. Sensing of COVID-19 Spike Protein in Nasopharyngeal Samples Using a Portable Surface Plasmon Resonance Diagnostic System. *Sens. Diagn.* **2022**. [CrossRef]
128. Moitra, P.; Chaichi, A.; Abid Hasan, S.M.; Dighe, K.; Alafeef, M.; Prasad, A.; Gartia, M.R.; Pan, D. Probing the Mutation Independent Interaction of DNA Probes with SARS-CoV-2 Variants through a Combination of Surface-Enhanced Raman Scattering and Machine Learning. *Biosens. Bioelectron.* **2022**, *208*, 114200. [CrossRef]
129. Bong, J.-H.; Kim, T.-H.; Jung, J.; Lee, S.J.; Sung, J.S.; Lee, C.K.; Kang, M.-J.; Kim, H.O.; Pyun, J.-C. Pig Sera-Derived Anti-SARS-CoV-2 Antibodies in Surface Plasmon Resonance Biosensors. *BioChip J.* **2020**, *14*, 358–368. [CrossRef]
130. Achadu, O.J.; Nwaji, N.; Lee, D.; Lee, J.; Akinoglu, E.M.; Giersig, M.; Park, E.Y. 3D Hierarchically Porous Magnetic Molybdenum Trioxide@gold Nanospheres as a Nanogap-Enhanced Raman Scattering Biosensor for SARS-CoV-2. *Nanoscale Adv.* **2022**, *4*, 871–883. [CrossRef]
131. Funari, R.; Chu, K.-Y.; Shen, A.Q. Detection of Antibodies against SARS-CoV-2 Spike Protein by Gold Nanospikes in an Opto-Microfluidic Chip. *Biosens. Bioelectron.* **2020**, *169*, 112578. [CrossRef] [PubMed]
132. Gutgsell, A.R.; Gunnarsson, A.; Forssén, P.; Gordon, E.; Fornstedt, T.; Geschwindner, S. Biosensor-Enabled Deconvolution of the Avidity-Induced Affinity Enhancement for the SARS-CoV-2 Spike Protein and ACE2 Interaction. *Anal. Chem.* **2022**, *94*, 1187–1194. [CrossRef] [PubMed]
133. Saad, Y.; Gazzah, M.H.; Mougin, K.; Selmi, M.; Belmabrouk, H. Sensitive Detection of SARS-CoV-2 Using a Novel Plasmonic Fiber Optic Biosensor Design. *Plasmonics* **2022**. [CrossRef]
134. Bistaffa, M.J.; Camacho, S.A.; Pazin, W.M.; Constantino, C.J.L.; Oliveira, O.N.; Aoki, P.H.B. Immunoassay Platform with Surface-Enhanced Resonance Raman Scattering for Detecting Trace Levels of SARS-CoV-2 Spike Protein. *Talanta* **2022**, *244*, 123381. [CrossRef] [PubMed]
135. Zhao, B.; Che, C.; Wang, W.; Li, N.; Cunningham, B.T. Single-Step, Wash-Free Digital Immunoassay for Rapid Quantitative Analysis of Serological Antibody against SARS-CoV-2 by Photonic Resonator Absorption Microscopy. *Talanta* **2021**, *225*, 122004. [CrossRef] [PubMed]
136. Cennamo, N.; Pasquardini, L.; Arcadio, F.; Lunelli, L.; Vanzetti, L.; Carafa, V.; Altucci, L.; Zeni, L. SARS-CoV-2 Spike Protein Detection through a Plasmonic D-Shaped Plastic Optical Fiber Aptasensor. *Talanta* **2021**, *233*, 122532. [CrossRef] [PubMed]
137. Zhang, Z.-Y.; Liu, X.; Shen, L.; Chen, L.; Fang, W.-H. Machine Learning with Multilevel Descriptors for Screening of Inorganic Nonlinear Optical Crystals. *J. Phys. Chem. C* **2021**, *125*, 25175–25188. [CrossRef]
138. Wang, X.; Wang, H.; Zhou, W.; Zhang, T.; Huang, H.; Song, Y.; Li, Y.; Liu, Y.; Kang, Z. Carbon Dots with Tunable Third-Order Nonlinear Coefficient Instructed by Machine Learning. *J. Photochem. Photobiol. A Chem.* **2022**, *426*, 113729. [CrossRef]
139. Fairbairn, C.E.; Kang, D.; Bosch, N. Using Machine Learning for Real-Time BAC Estimation from a New-Generation Transdermal Biosensor in the Laboratory. *Drug Alcohol Depend.* **2020**, *216*, 108205. [CrossRef]
140. Robison, H.M.; Chapman, C.A.; Zhou, H.; Erskine, C.L.; Theel, E.; Peikert, T.; Lindestam Arlehamn, C.S.; Sette, A.; Bushell, C.; Welge, M.; et al. Risk Assessment of Latent Tuberculosis Infection through a Multiplexed Cytokine Biosensor Assay and Machine Learning Feature Selection. *Sci. Rep.* **2021**, *11*, 20544. [CrossRef]
141. Kim, H.; Seong, W.; Rha, E.; Lee, H.; Kim, S.K.; Kwon, K.K.; Park, K.-H.; Lee, D.-H.; Lee, S.-G. Machine Learning Linked Evolutionary Biosensor Array for Highly Sensitive and Specific Molecular Identification. *Biosens. Bioelectron.* **2020**, *170*, 112670. [CrossRef] [PubMed]
142. Pennacchio, A.; Giampaolo, F.; Piccialli, F.; Cuomo, S.; Notomista, E.; Spinelli, M.; Amoresano, A.; Piscitelli, A.; Giardina, P. A Machine Learning-Enhanced Biosensor for Mercury Detection Based on an Hydrophobin Chimera. *Biosens. Bioelectron.* **2022**, *196*, 113696. [CrossRef] [PubMed]
143. Green, E.M.; van Mourik, R.; Wolfus, C.; Heitner, S.B.; Dur, O.; Semigran, M.J. Machine Learning Detection of Obstructive Hypertrophic Cardiomyopathy Using a Wearable Biosensor. *Npj Digit. Med.* **2019**, *2*, 57. [CrossRef]

144. Vakilian, K.A. A Nitrate Enzymatic Biosensor Based on Optimized Machine Learning Techniques. In *2022 9th Iranian Joint Congress on Fuzzy and Intelligent Systems (CFIS)*; IEEE: Piscataway, NJ, USA, 2022; p. 21758368.

145. Khor, S.M.; Choi, J.; Won, P.; Ko, S.H. Challenges and Strategies in Developing an Enzymatic Wearable Sweat Glucose Biosensor as a Practical Point-Of-Care Monitoring Tool for Type II Diabetes. *Nanomaterials* **2022**, *12*, 221. [CrossRef] [PubMed]

146. Gonzalez-Navarro, F.; Stilianova-Stoytcheva, M.; Renteria-Gutierrez, L.; Belanche-Muñoz, L.; Flores-Rios, B.; Ibarra-Esquer, J. Glucose Oxidase Biosensor Modeling and Predictors Optimization by Machine Learning Methods. *Sensors* **2016**, *16*, 1483. [CrossRef] [PubMed]

147. Boscolo, S.; Finot, C. Artificial Neural Networks for Nonlinear Pulse Shaping in Optical Fibers. *Opt. Laser Technol.* **2020**, *131*, 106439. [CrossRef]

148. Chicea, D.; Rei, S.M. A Fast Artificial Neural Network Approach for Dynamic Light Scattering Time Series Processing. *Meas. Sci. Technol.* **2018**, *29*, 105201. [CrossRef]

149. Talebi-Moghaddam, S.; Bauer, F.J.; Huber, F.J.T.; Will, S.; Daun, K.J. Inferring Soot Morphology through Multi-Angle Light Scattering Using an Artificial Neural Network. *J. Quant. Spectrosc. Radiat. Transf.* **2020**, *251*, 106957. [CrossRef]

150. Pelenis, D.; Barauskas, D.; Vanagas, G.; Dzikaras, M.; Viržonis, D. CMUT-Based Biosensor with Convolutional Neural Network Signal Processing. *Ultrasonics* **2019**, *99*, 105956. [CrossRef]

151. Byun, S.-J.; Kim, D.-G.; Park, K.-D.; Choi, Y.-J.; Kumar, P.; Ali, I.; Kim, D.-G.; Yoo, J.-M.; Huh, H.-K.; Jung, Y.-J.; et al. A Low-Power Analog Processor-in-Memory-Based Convolutional Neural Network for Biosensor Applications. *Sensors* **2022**, *22*, 4555. [CrossRef]

152. Mennel, L.; Symonowicz, J.; Wachter, S.; Polyushkin, D.K.; Molina-Mendoza, A.J.; Mueller, T. Ultrafast Machine Vision with 2D Material Neural Network Image Sensors. *Nature* **2020**, *579*, 62–66. [CrossRef] [PubMed]

153. Chen, C.; Wang, J. Optical Biosensors: An Exhaustive and Comprehensive Review. *Analyst* **2020**, *145*, 1605–1628. [CrossRef] [PubMed]

154. Yan, Y.; Gong, J.; Chen, J.; Zeng, Z.; Huang, W.; Pu, K.; Liu, J.; Chen, P. Recent Advances on Graphene Quantum Dots: From Chemistry and Physics to Applications. *Adv. Mater.* **2019**, *31*, 1808283. [CrossRef]

155. Zhao, Y.; Li, Y.; Zhang, P.; Yan, Z.; Zhou, Y.; Du, Y.; Qu, C.; Song, Y.; Zhou, D.; Qu, S.; et al. Cell-Based Fluorescent Microsphere Incorporated with Carbon Dots as a Sensitive Immunosensor for the Rapid Detection of Escherichia Coli O157 in Milk. *Biosens. Bioelectron.* **2021**, *179*, 113057. [CrossRef]

156. Hu, Q.; Wang, S.; Duan, H.; Liu, Y. A Fluorescent Biosensor for Sensitive Detection of Salmonella Typhimurium Using Low-Gradient Magnetic Field and Deep Learning via Faster Region-Based Convolutional Neural Network. *Biosensors* **2021**, *11*, 447. [CrossRef] [PubMed]

157. Zhu, X.; Liu, P.; Xue, T.; Ge, Y.; Ai, S.; Sheng, Y.; Wu, R.; Xu, L.; Tang, K.; Wen, Y. A Novel Graphene-like Titanium Carbide MXene/Au–Ag Nanoshuttles Bifunctional Nanosensor for Electrochemical and SERS Intelligent Analysis of Ultra-Trace Carbendazim Coupled with Machine Learning. *Ceram. Int.* **2021**, *47*, 173–184. [CrossRef]

158. Chen, G.; Du, J.; Sun, L.; Zhang, W.; Xu, K.; Chen, X.; Reed, G.T.; He, Z. Nonlinear Distortion Mitigation by Machine Learning of SVM Classification for PAM-4 and PAM-8 Modulated Optical Interconnection. *J. Light. Technol.* **2018**, *36*, 650–657. [CrossRef]

159. Lin, J.; Shen, G.; Zhai, Z.; Zheng, D.; Li, Y.; Chang, Z.; Zong, L.; Deng, N.; Chang, T. Delivering Distributed Machine Learning Services in All-Optical Datacenter Networks with Torus Topology. In *Asia Communications and Photonics Conference 2021*; Chang-Hasnain Willner, A., Shieh, W., Shum, P., Su, Y., Li, G., Eggleton, B., Essiambre, R., Dai, D., Ma, D.C., Eds.; Optica Publishing Group: Washington, DC, USA, 2021; p. W3C.5.

160. McConnon, A. Deep Learning Characterizes Optical Pulses Using Speckle Patterns at the End of Multimode Fibers. *Scilight* **2020**, *2020*, 381102. [CrossRef]

161. Noble, J.; Zhou, C.; Murray, W.T.; Liu, Z. Convolutional Neural Network Reconstruction of Ultrashort Optical Pulses. *Ultrafast Nonlinear Imaging Spectrosc. VIII* **2020**, *11497*, 20. [CrossRef]

162. Närhi, M.; Salmela, L.; Toivonen, J.; Billet, C.; Dudley, J.M.; Genty, G. Machine Learning Analysis of Extreme Events in Optical Fibre Modulation Instability. *Nat. Commun.* **2018**, *9*, 4923. [CrossRef]

163. Kokhanovskiy, A.; Kuprikov, E.; Bednyakova, A.; Popkov, I.; Smirnov, S.; Turitsyn, S. Inverse Design of Mode-Locked Fiber Laser by Particle Swarm Optimization Algorithm. *Sci. Rep.* **2021**, *11*, 13555. [CrossRef] [PubMed]

164. Woodward, R.I.; Kelleher, E.J.R. Towards 'Smart Lasers': Self-Optimisation of an Ultrafast Pulse Source Using a Genetic Algorithm. *Sci. Rep.* **2016**, *6*, 37616. [CrossRef] [PubMed]

165. Zahavy, T.; Dikopoltsev, A.; Moss, D.; Haham, G.I.; Cohen, O.; Mannor, S.; Segev, M. Deep Learning Reconstruction of Ultrashort Pulses. *Optica* **2018**, *5*, 666. [CrossRef]

166. Underwood, K.J.; Jones, A.M.; Gopinath, J.T. Synthesis of Coherent Optical Pulses Using a Field-Programmable Gate Array (FPGA)-Based Gradient Descent Phase-Locking Algorithm with Three Semiconductor Lasers. In *CLEO: 2015*; OSA: Washington, DC, USA, 2015; p. 15380458.

167. Wang, D.; Zhang, M.; Cai, Z.; Cui, Y.; Li, Z.; Han, H.; Fu, M.; Luo, B. Combatting Nonlinear Phase Noise in Coherent Optical Systems with an Optimized Decision Processor Based on Machine Learning. *Opt. Commun.* **2016**, *369*, 199–208. [CrossRef]

168. Marciniak, M. Two-Beam-Propagation Method Algorithm for Second-Harmonic Generation in Dielectric Planar Waveguides. In *Proceedings of SPIE*; Tuchin, V.V., Ryabukho, V.P., Zimnyakov, D.A., Eds.; SPIE: Bellingham, WA, USA, 1999; Volume 3726, p. 32.

169. Andrews, D.L.; Romero, L.C.D.; Meath, W.J. An Algorithm for the Nonlinear Optical Susceptibilities of Dipolar Molecules, and an Application to Third Harmonic Generation. *J. Phys. B At. Mol. Opt. Phys.* **1999**, *32*, 1. [CrossRef]

170. Kurokawa, Y.; Nomura, S.; Takemori, T.; Aoyagi, Y. Fast Algorithm for Calculating Two-Photon Absorption Spectra. *Phys. Rev. E* **1999**, *59*, 3694–3697. [CrossRef]

171. Boynton, G.C.; Gordon, H.R. Irradiance Inversion Algorithm for Estimating the Absorption and Backscattering Coefficients of Natural Waters: Raman-Scattering Effects. *Appl. Opt.* **2000**, *39*, 3012–3022. [CrossRef]

172. Lin, F.; Gong, Y.; Shum, P. Optimization Design By Genetic Algorithm With A New Crossover Method For Broadband Fiber Raman Amplifiers. In *Optical Communications and Networks*; World Scientific: Singapore, 2002; pp. 249–252, ISBN 978-981-238-232-0.

173. Hamza, M.Y.; Tariq, S.; Awais, M.M.; Yang, S. Mitigation of the Effects of Self Phase Modulation and Group-Velocity Dispersion in Fiber Optic Communications: Dispersion- and Power-Map Cooptimization Using the Genetic Algorithm. *Opt. Eng.* **2008**, *47*, 1–12. [CrossRef]

174. Ohto, T.; Usui, K.; Hasegawa, T.; Bonn, M.; Nagata, Y. Toward Ab Initio Molecular Dynamics Modeling for Sum-Frequency Generation Spectra; an Efficient Algorithm Based on Surface-Specific Velocity-Velocity Correlation Function. *J. Chem. Phys.* **2015**, *143*, 124702. [CrossRef]

175. Hakimian, F.; Shayesteh, M.R.; Moslemi, M.R. Optimization of Four-Wave Mixing Wavelength Conversion in a Quantum-Dot Semiconductor Optical Amplifier Based on the Genetic Algorithm. *Opt. Quantum Electron.* **2021**, *53*, 140. [CrossRef]

176. Al-Qarni, A.A.; Bakodah, H.O.; Alshaery, A.A.; Biswas, A.; Yıldırım, Y.; Moraru, L.; Moldovanu, S. Numerical Simulation of Cubic-Quartic Optical Solitons with Perturbed Fokas–Lenells Equation Using Improved Adomian Decomposition Algorithm. *Mathematics* **2022**, *10*, 138. [CrossRef]

177. Moreno-Larios, J.A.; Ramírez-Guerra, C.; Contreras-Martínez, R.; Rosete-Aguilar, M.; Garduño-Mejía, J. Algorithm to Filter the Noise in the Spectral Intensity of Ultrashort Laser Pulses. *Appl. Opt.* **2020**, *59*, 7233–7241. [CrossRef] [PubMed]

178. Fan, Q.; Zhou, G.; Gui, T.; Lu, C.; Lau, A.P.T. Advancing Theoretical Understanding and Practical Performance of Signal Processing for Nonlinear Optical Communications through Machine Learning. *Nat. Commun.* **2020**, *11*, 3694. [CrossRef] [PubMed]

179. Smolyaninov, I.I. Nonlinear Optics of Photonic Hyper-Crystals: Optical Limiting and Hyper-Computing. *J. Opt. Soc. Am. B* **2019**, *36*, 1629–1636. [CrossRef]

180. Dikopoltsev, A.; Zahavy, T.; Ziv, R.; Rubinstein, I.; Sidorenko, P.; Mannor, S.; Cohen, O.; Segev, M. Reconstruction of Ultrashort Pulses Using Deep Neural Networks. In *2018 2nd URSI Atlantic Radio Science Meeting (AT-RASC)*; IEEE: Piscataway, NJ, USA, 2018; p. 18144568.

181. Wang, Q.; Liu, W.; Chen, X.; Wang, X.; Chen, G.; Zhu, X. Quantification of Scar Collagen Texture and Prediction of Scar Development via Second Harmonic Generation Images and a Generative Adversarial Network. *Biomed. Opt. Express* **2021**, *12*, 5305–5319. [CrossRef] [PubMed]

182. Wang, G.; Sun, Y.; Jiang, S.; Wu, G.; Liao, W.; Chen, Y.; Lin, Z.; Liu, Z.; Zhuo, S. Machine Learning-Based Rapid Diagnosis of Human Borderline Ovarian Cancer on Second-Harmonic Generation Images. *Biomed. Opt. Express* **2021**, *12*, 5658–5669. [CrossRef]

183. Wu, B.; Judd, N.B.; Smith, J.T.; Icaza, M.; Mukherjee, S.; Jain, M.; Gallagher, R.M.; Szeligowski, R.V. A Pilot Study for Distinguishing Chromophobe Renal Cell Carcinoma and Oncocytoma Using Second Harmonic Generation Imaging and Convolutional Neural Network Analysis of Collagen Fibrillar Structure. In *Optical Biopsy XVI: Toward Real-Time Spectroscopic Imaging and Diagnosis*; Alfano, R.R., Demos, S.G., Eds.; SPIE: Bellingham, WA, USA, 2018; Volume 10489, p. 44.

184. Vidal-Codina, F.; Nguyen, N.-C.; Ciracì, C.; Oh, S.-H.; Peraire, J. A Nested Hybridizable Discontinuous Galerkin Method for Computing Second-Harmonic Generation in Three-Dimensional Metallic Nanostructures. *J. Comput. Phys.* **2021**, *429*, 110000. [CrossRef]

185. Xu, Z.; Wang, P.; Zhao, M.; Yang, M.; Zhao, W.; Hu, K.; Dong, L.; Wang, S.; Li, X.; Yang, P.; et al. Prediction of Second-Harmonic Generation Wave-Front Distribution by Extreme Learning Machine. *IEEE Photonics Technol. Lett.* **2020**, *32*, 693–696. [CrossRef]

186. Jafari, R.; Jones, T.; Trebino, R. 100% Reliable Algorithm for Second-Harmonic-Generation Frequency-Resolved Optical Gating. *Opt. Express* **2019**, *27*, 2112–2124. [CrossRef]

187. Jafari, R.; Jones, T.; Trebino, R. 100% Reliable Frequency-Resolved-Optical-Gating Pulse Retrieval Algorithmic Approach. In *Frontiers in Optics + Laser Science APS/DLS*; OSA: Washington, DC, USA, 2019; p. JW3A.33.

188. Saito, K.; Tanabe, T.; Oyama, Y. Numerical Analysis of Second Harmonic Generation for THz-Wave in a Photonic Crystal Waveguide Using a Nonlinear FDTD Algorithm. *Opt. Commun.* **2016**, *365*, 164–167. [CrossRef]

189. Schneidereit, D.; Nübler, S.; Prölß, G.; Reischl, B.; Schürmann, S.; Müller, O.J.; Friedrich, O. Optical Prediction of Single Muscle Fiber Force Production Using a Combined Biomechatronics and Second Harmonic Generation Imaging Approach. *Light Sci. Appl.* **2018**, *7*, 79. [CrossRef] [PubMed]

190. Liu, Q.; Mukhopadhyay, S.; Bastidas Rodriguez, M.X.; Fu, X.; Sahu, S.; Burk, D.; Gartia, M. A One-Shot Learning Framework for Assessment of Fibrillar Collagen from Second Harmonic Generation Images of an Infarcted Myocardium. In *2020 IEEE 17th International Symposium on Biomedical Imaging (ISBI)*; IEEE: Piscataway, NJ, USA, 2020; pp. 839–843.

191. Diatta, A.; Rouquette, J.; Armand, P.; Hermet, P. Density Functional Theory Prediction of the Second Harmonic Generation and Linear Pockels Effect in Trigonal BaZnO$_2$. *J. Phys. Chem. C* **2018**, *122*, 21277–21283. [CrossRef]

192. Comin, A.; Hartschuh, A. Efficient Optimization of SHG Hotspot Switching in Plasmonic Nanoantennas Using Phase-Shaped Laser Pulses Controlled by Neural Networks. *Opt. Express* **2018**, *26*, 33678–33686. [CrossRef] [PubMed]

193. Hall, G.; Liang, W.; Li, X. Efficient and Unbiased Fit-Free Algorithm for Quantification of Collagen Fiber Alignment for SHG Imaging Applications. In *Biomedical Optics 2016*; OSA: Washington, DC, USA, 2016.

194. Preißler, D.; Kiefer, D.; Führer, T.; Walther, T. Evolutionary Algorithm-Assisted Design of a UV SHG Cavity with Elliptical Focusing to Avoid Crystal Degradation. *Appl. Phys. B* **2019**, *125*, 220. [CrossRef]

195. Hall, G.; Liang, W.; Li, X. Fitting-Free Algorithm for Efficient Quantification of Collagen Fiber Alignment in SHG Imaging Applications. *Biomed. Opt. Express* **2017**, *8*, 4609–4620. [CrossRef]

196. Kang, L.; Liang, F.; Gong, P.; Lin, Z.; Liu, F.; Huang, B. Two Novel Deep-Ultraviolet Nonlinear Optical Crystals with Shorter Phase-Matching Second Harmonic Generation than KBe2BO3F2: A First-Principles Prediction. *Phys. Status Solidi–Rapid Res. Lett.* **2018**, *12*, 1800276. [CrossRef]

197. Zhang, B.; Tikhonov, E.; Xie, C.; Yang, Z.; Pan, S. Prediction of Fluorooxoborates with Colossal Second Harmonic Generation (SHG) Coefficients and Extremely Wide Band Gaps: Towards Modulating Properties by Tuning the BO_3/BO_3F Ratio in Layers. *Angew. Chem.* **2019**, *131*, 11852–11856. [CrossRef]

198. McLean, J.; DiMarzio, C. A Linear Algorithm for Quantitative Measure of Corneal Collagen Fiber Orientation Using Second Harmonic Generation Microscopy. *Proc. SPIE* **2016**, *9713*, 971317. [CrossRef]

199. Kumar, A.; Yadav, M.P.S. Computational Studies of Third-Order Nonlinear Optical Properties of Pyridine Derivative 2-Aminopyridinium p-Toluenesulphonate Crystal. *Pramana* **2017**, *89*, 7. [CrossRef]

200. Salem, M.A.; Twelves, I.; Brown, A. Prediction of Two-Photon Absorption Enhancement in Red Fluorescent Protein Chromophores Made from Non-Canonical Amino Acids. *Phys. Chem. Chem. Phys.* **2016**, *18*, 24408–24416. [CrossRef]

201. Eybposh, M.H.; Caira, N.W.; Atisa, M.; Chakravarthula, P.; Pégard, N.C. Enhanced Two-Photon Absorption with Deep Learning-Based Computer Generated Holography. In *Frontiers in Optics/Laser Science*; Lee Mazzali, C., Corwin, K., Jason Jones, R.B., Eds.; OSA: Washington, DC, USA, 2020.

202. Deng, A.; Huang, J.; Liu, H.; Cai, W. Deep Learning Algorithms for Temperature Field Reconstruction of Nonlinear Tomographic Absorption Spectroscopy. *Meas. Sens.* **2020**, *10–12*, 100024. [CrossRef]

203. Yadav, C.; Roy, S. Ultrafast Nonlinear Absorption in Hemoprotein Cytochrome-c and Its Application to Computing. *Opt. Quantum Electron.* **2016**, *48*, 377. [CrossRef]

204. Wang, Z.; Zhu, N.; Wang, W.; Chao, X. Y-Net: A Dual-Branch Deep Learning Network for Nonlinear Absorption Tomography with Wavelength Modulation Spectroscopy. *Opt. Express* **2022**, *30*, 2156–2172. [CrossRef] [PubMed]

205. Neskorniuk, V.; Freire, P.J.; Napoli, A.; Spinnler, B.; Schairer, W.; Prilepsky, J.E.; Costa, N.; Turitsyn, S.K. Simplifying the Supervised Learning of Kerr Nonlinearity Compensation Algorithms by Data Augmentation. In *2020 European Conference on Optical Communications (ECOC)*; IEEE: Piscataway, NJ, USA, 2020; pp. 1–4.

206. Yıldırım, Y.; Çelik, N.; Yaşar, E. Nonlinear Schrödinger Equations with Spatio-Temporal Dispersion in Kerr, Parabolic, Power and Dual Power Law Media: A Novel Extended Kudryashov's Algorithm and Soliton Solutions. *Results Phys.* **2017**, *7*, 3116–3123. [CrossRef]

207. Solli, D.R.; Ropers, C.; Koonath, P.; Jalali, B. Optical Rogue Waves. *Nature* **2007**, *450*, 1054–1057. [CrossRef]

208. Gopalakrishnan, S.S.; Panajotov, K.; Taki, M.; Tlidi, M. Dissipative Light Bullets in Kerr Cavities: Multistability, Clustering, and Rogue Waves. *Phys. Rev. Lett.* **2021**, *126*, 153902. [CrossRef]

209. Jhangeer, A.; Faridi, W.A.; Asjad, M.I.; Akgül, A. Analytical Study of Soliton Solutions for an Improved Perturbed Schrödinger Equation with Kerr Law Non-Linearity in Non-Linear Optics by an Expansion Algorithm. *Partial Differ. Equ. Appl. Math.* **2021**, *4*, 100102. [CrossRef]

210. Chase, H.M.; Rudshteyn, B.; Psciuk, B.T.; Upshur, M.A.; Strick, B.F.; Thomson, R.J.; Batista, V.S.; Geiger, F.M. Assessment of DFT for Computing Sum Frequency Generation Spectra of an Epoxydiol and a Deuterated Isotopologue at Fused Silica/Vapor Interfaces. *J. Phys. Chem. B* **2016**, *120*, 1919–1927. [CrossRef]

211. Shah, S.A.; Pikalov, A.A.; Baldelli, S. ChemSpecNet: A Neural Network for Chemical Analysis of Sum Frequency Generation Spectroscopic Imaging. *Opt. Commun.* **2022**, *507*, 127691. [CrossRef]

212. Jackson, W.; Zishan, W.; Xiong, W. Imaging Orientation of a Single Molecular Hierarchical Self-Assembled Sheet: The Combined Power of a Vibrational Sum Frequency Generation Microscopy and Neural Network. *ChemRxiv* **2022**. [CrossRef]

213. Cai, M.; Zhuge, Q.; Lun, H.; Fu, M.; Yi, L.; Hu, W. Pilot-Aided Self-Phase Modulation Noise Monitoring Based on Artificial Neural Network. In *Asia Communications and Photonics Conference (ACPC) 2019*; Optica Publishing Group: Chengdu, China, 2019; p. M4A.9.

214. Fumumoto, Y.; Owaki, S.; Nakamura, M. Effect of Number of Neurons of a Neural-Network on Compensation Performance of SPM Non-Linear Waveform Distortion. In *2017 Opto-Electronics and Communications Conference (OECC) and Photonics Global Conference (PGC)*; IEEE: Piscataway, NJ, USA, 2017; pp. 1–2.

215. Owaki, S.; Nakamura, M. Simultaneous Compensation of Waveform Distortion Caused by Chromatic Dispersion and SPM Using a Three-Layer Neural-Network. In *2017 Opto-Electronics and Communications Conference (OECC) and Photonics Global Conference (PGC)*; IEEE: Piscataway, NJ, USA, 2017; p. 17373621.

216. Caballero, F.J.V.; Ives, D.J.; Laperle, C.; Charlton, D.; Zhuge, Q.; O'Sullivan, M.; Savory, S.J. Machine Learning Based Linear and Nonlinear Noise Estimation. *J. Opt. Commun. Netw.* **2018**, *10*, 42–51. [CrossRef]

217. Brusin, A.M.R.; de Moura, U.C.; Curri, V.; Zibar, D.; Carena, A. Introducing Load Aware Neural Networks for Accurate Predictions of Raman Amplifiers. *J. Light. Technol.* **2020**, *38*, 6481–6491. [CrossRef]

218. Soltani, M.; Da Ros, F.; Carena, A.; Zibar, D. Spectral and Spatial Power Evolution Design With Machine Learning-Enabled Raman Amplification. *J. Light. Technol.* **2022**, *40*, 3546–3556. [CrossRef]

219. Soltani, M.; Da Ros, F.; Carena, A.; Zibar, D. Distance and Spectral Power Profile Shaping Using Machine Learning Enabled Raman Amplifiers. In *2021 IEEE Photonics Society Summer Topicals Meeting Series (SUM)*; IEEE: Piscataway, NJ, USA, 2021; p. 21048928.

220. de Moura, U.C.; Da Ros, F.; Zibar, D.; Rosa Brusin, A.M.; Carena, A. Optimization of Raman Amplifiers Using Machine Learning. In *2021 IEEE Photonics Society Summer Topicals Meeting Series (SUM)*; IEEE: Piscataway, NJ, USA, 2021; p. 21048937.

221. Marcon, G.; Galtarossa, A.; Palmieri, L.; Santagiustina, M. Model-Aware Deep Learning Method for Raman Amplification in Few-Mode Fibers. *J. Light. Technol.* **2021**, *39*, 1371–1380. [CrossRef]

222. Huang, Y.; Du, J.; Chen, Y.; Xu, K.; He, Z. Machine Learning Assisted Inverse Design for Ultrafine, Dynamic and Arbitrary Gain Spectrum Shaping of Raman Amplification. *Photonics* **2021**, *8*, 260. [CrossRef]

223. Ionescu, M.; Ghazisaeidi, A.; Renaudier, J. Machine Learning Assisted Hybrid EDFA-Raman Amplifier Design for C+L Bands. In Proceedings of the 2020 European Conference on Optical Communications (ECOC), Virtual Event, 6–10 December 2020; IEEE: Piscataway, NJ, USA, 2020; p. 20349557.

224. Marcon, G.; Galtarossa, A.; Palmieri, L.; Santagiustina, M. C+L Band Gain Design in Few-Mode Fibers Using Raman Amplification and Machine Learning. In *2020 Italian Conference on Optics and Photonics (ICOP)*; IEEE: Piscataway, NJ, USA, 2020; p. 20264995.

225. Soltani, M.; Da Ros, F.; Carena, A.; Zibar, D. Inverse Design of a Raman Amplifier in Frequency and Distance Domains Using Convolutional Neural Networks. *Opt. Lett.* **2021**, *46*, 2650–2653. [CrossRef]

226. Zibar, D.; de Moura, U.C.; Rosa Brusin, A.M.; Carena, A.; Da Ros, F. Machine Learning Enabled Raman Amplifiers. In Proceedings of the 2021 Conference on Lasers and Electro-Optics Europe and European Quantum Electronics Conference, Virtual Event, 21–25 June 2021; Optica Publishing Group: Munich, Germany, 2021; p. ci_1_3.

227. Marcon, G.; Galtarossa, A.; Palmieri, L.; Santagiustina, M. Gain Design of Few-Mode Fiber Raman Amplifiers Using an Autoencoder-Based Machine Learning Approach. In *2020 European Conference on Optical Communications (ECOC)*; IEEE: Piscataway, NJ, USA, 2020; p. 20349595.

228. Gong, J.; Liu, F.; Wu, Y.; Zhang, Y.; Lei, S.; Zhu, Z. Raman Fiber Amplifier Design Scheme Based on Back Propagation Neural Network Algorithm. *Opt. Eng.* **2021**, *60*, 37103. [CrossRef]

229. Hunter, R.A.; Asare-Werehene, M.; Mandour, A.; Tsang, B.K.; Anis, H. Determination of Chemoresistance in Ovarian Cancer by Simultaneous Quantification of Exosomes and Exosomal Cisplatin with Surface Enhanced Raman Scattering. *Sens. Actuators B Chem.* **2022**, *354*, 131237. [CrossRef]

230. Chen, T.; Cheng, Q.; Lee, H.J. Machine-Learning-Mediated Single-Cell Classification by Hyperspectral Stimulated Raman Scattering Imaging. *Opt. Heal. Care Biomed. Opt. XI* **2021**, *11900*, 30. [CrossRef]

231. Viljoen, R.; Neethling, P.; Spangenberg, D.; Heidt, A.; Frey, H.-M.; Feurer, T.; Rohwer, E. Implementation of Temporal Ptychography Algorithm, I2PIE, for Improved Single-Beam Coherent Anti-Stokes Raman Scattering Measurements. *J. Opt. Soc. Am. B* **2020**, *37*, A259–A265. [CrossRef]

232. Melnikov, G.; Ignatenko, N.; Petrova, L.; Manzhos, O.; Gromkov, A. On the Influence of Clustering Processes in the Liquid Structure on Raman Scattering. *MATEC Web Conf.* **2021**, *344*, 01010. [CrossRef]

233. Fang, X.; Zeng, Q.; Yan, X.; Zhao, Z.; Chen, N.; Deng, Q.; Zhu, M.; Zhang, Y.; Li, S. Fast Discrimination of Tumor and Blood Cells by Label-Free Surface-Enhanced Raman Scattering Spectra and Deep Learning. *J. Appl. Phys.* **2021**, *129*, 123103. [CrossRef]

234. Weng, S.; Xu, X.; Li, J.; Wong, S.T.C. Combining Deep Learning and Coherent Anti-Stokes Raman Scattering Imaging for Automated Differential Diagnosis of Lung Cancer. *J. Biomed. Opt.* **2017**, *22*, 106017. [CrossRef] [PubMed]

235. Yamato, N.; Matsuya, M.; Niioka, H.; Miyake, J.; Hashimoto, M. Nerve Segmentation with Deep Learning from Label-Free Endoscopic Images Obtained Using Coherent Anti-Stokes Raman Scattering. *Biomolecules* **2020**, *10*, 1012. [CrossRef] [PubMed]

236. Brusin, A.M.R.; Zefreh, M.R.; Poggiolini, P.; Piciaccia, S.; Forghieri, F.; Carena, A. Machine Learning for Power Profiles Prediction in Presence of Inter-Channel Stimulated Raman Scattering. In *2021 European Conference on Optical Communication (ECOC)*; IEEE: Piscataway, NJ, USA, 2021; p. 21549326.

237. Yamato, N.; Niioka, H.; Miyake, J.; Hashimoto, M. Improvement of Nerve Imaging Speed with Coherent Anti-Stokes Raman Scattering Rigid Endoscope Using Deep-Learning Noise Reduction. *Sci. Rep.* **2020**, *10*, 15212. [CrossRef]

238. Yin, P.; Li, G.; Zhang, B.; Farjana, H.; Zhao, L.; Qin, H.; Hu, B.; Ou, J.; Tian, J. Facile PEG-Based Isolation and Classification of Cancer Extracellular Vesicles and Particles with Label-Free Surface-Enhanced Raman Scattering and Pattern Recognition Algorithm. *Analyst* **2021**, *146*, 1949–1955. [CrossRef]

239. Shi, H.; Wang, H.; Meng, X.; Chen, R.; Zhang, Y.; Su, Y.; He, Y. Setting Up a Surface-Enhanced Raman Scattering Database for Artificial-Intelligence-Based Label-Free Discrimination of Tumor Suppressor Genes. *Anal. Chem.* **2018**, *90*, 14216–14221. [CrossRef]

240. Sun, Y.W.; Liu, C.; Chan, K.L.; Xie, P.H.; Liu, W.Q.; Zeng, Y.; Wang, S.M.; Huang, S.H.; Chen, J.; Wang, Y.P.; et al. Stack Emission Monitoring Using Non-Dispersive Infrared Spectroscopy with an Optimized Nonlinear Absorption Cross Interference Correction Algorithm. *Atmos. Meas. Tech.* **2013**, *6*, 1993–2005. [CrossRef]

241. Leong, Y.X.; Lee, Y.H.; Koh, C.S.L.; Phan-Quang, G.C.; Han, X.; Phang, I.Y.; Ling, X.Y. Surface-Enhanced Raman Scattering (SERS) Taster: A Machine-Learning-Driven Multireceptor Platform for Multiplex Profiling of Wine Flavors. *Nano Lett.* **2021**, *21*, 2642–2649. [CrossRef]

242. Buzalewicz, I.; Suchwałko, A.; Karwańska, M.; Wieliczko, A.; Podbielska, H. Development of the Correction Algorithm to Limit the Deformation of Bacterial Colonies Diffraction Patterns Caused by Misalignment and Its Impact on the Bacteria Identification in the Proposed Optical Biosensor. *Sensors* **2020**, *20*, 5797. [CrossRef]

243. Hu, J.; Ma, L.; Wang, S.; Yang, J.; Chang, K.; Hu, X.; Sun, X.; Chen, R.; Jiang, M.; Zhu, J.; et al. Biomolecular Interaction Analysis Using an Optical Surface Plasmon Resonance Biosensor: The Marquardt Algorithm vs Newton Iteration Algorithm. *PLoS ONE* **2015**, *10*, e0132098. [CrossRef] [PubMed]

244. Mirsanaye, K.; Uribe Castaño, L.; Kamaliddin, Y.; Golaraei, A.; Augulis, R.; Kontenis, L.; Done, S.J.; Žurauskas, E.; Stambolic, V.; Wilson, B.C.; et al. Machine Learning-Enabled Cancer Diagnostics with Widefield Polarimetric Second-Harmonic Generation Microscopy. *Sci. Rep.* **2022**, *12*, 10290. [CrossRef] [PubMed]

245. Desa, D.E.; Strawderman, R.L.; Wu, W.; Hill, R.L.; Smid, M.; Martens, J.W.M.; Turner, B.M.; Brown, E.B. Intratumoral Heterogeneity of Second-Harmonic Generation Scattering from Tumor Collagen and Its Effects on Metastatic Risk Prediction. *BMC Cancer* **2020**, *20*, 1217. [CrossRef]

246. Jafari, R.; Jones, T.; Trebino, R. 100% Robust and Fast Algorithm for Second-Harmonic-Generation Frequency-Resolved Optical Gating. *Real-Time Meas. Rogue Phenom. Single-Shot Appl. IV SPIE LASE* **2019**, *10903*, 22. [CrossRef]

247. Tan, T.; Peng, C.; Yuan, Z.; Xie, X.; Liu, H.; Xie, Z.; Huang, S.-W.; Rao, Y.; Yao, B. Predicting Kerr Soliton Combs in Microresonators via Deep Neural Networks. *J. Light. Technol.* **2020**, *38*, 6591–6599. [CrossRef]

248. Costa, C.; Borges, L.; Penchel, R.A.; Abbade, M.L.F.; Giacoumidis, E.; Wei, J.; de Oliveira, J.A.; Santos, M.; Marconi, J.D.; Pita, J.L.; et al. Self-Phase Modulation and Inter-Polarization Cross-Phase Modulation Mitigation in Single-Channel Dp-16qam Coherent Pon Employing 4d Clustering. *SSRN Electron. J.* **2022**. [CrossRef]

249. Chen, Y.; Du, J.; Huang, Y.; Xu, K.; He, Z. Intelligent Gain Flattening in Wavelength and Space Domain for FMF Raman Amplification by Machine Learning Based Inverse Design. *Opt. Express* **2020**, *28*, 11911–11920. [CrossRef]

250. Chen, Y.; Du, J.; Huang, Y.; Xu, K.; He, Z. Intelligent Gain Flattening of FMF Raman Amplification by Machine Learning Based Inverse Design. In Proceedings of the Optical Fiber Communication Conference (OFC) 2020, San Diego, CA, USA, 8–12 March 2020; Optica Publishing Group: San Diego, CA, USA, 2020; p. T4B.1.

251. Jiang, L.; Mehedi Hassan, M.; Jiao, T.; Li, H.; Chen, Q. Rapid Detection of Chlorpyrifos Residue in Rice Using Surface-Enhanced Raman Scattering Coupled with Chemometric Algorithm. *Spectrochim. Acta Part A Mol. Biomol. Spectrosc.* **2021**, *261*, 119996. [CrossRef]

252. Li, H.; Mehedi Hassan, M.; Wang, J.; Wei, W.; Zou, M.; Ouyang, Q.; Chen, Q. Investigation of Nonlinear Relationship of Surface Enhanced Raman Scattering Signal for Robust Prediction of Thiabendazole in Apple. *Food Chem.* **2021**, *339*, 127843. [CrossRef]

253. Lussier, F.; Missirlis, D.; Spatz, J.P.; Masson, J.-F. Machine-Learning-Driven Surface-Enhanced Raman Scattering Optophysiology Reveals Multiplexed Metabolite Gradients Near Cells. *ACS Nano* **2019**, *13*, 1403–1411. [CrossRef]

254. Burzynski, N.; Yuan, Y.; Felsen, A.; Reitano, D.; Wang, Z.; Sethi, K.A.; Lu, F.; Chiu, K. Deep Learning Techniques for Unmixing of Hyperspectral Stimulated Raman Scattering Images. In *2021 IEEE International Conference on Big Data (Big Data)*; IEEE: Piscataway, NJ, USA, 2021; pp. 5862–5864.

255. Fang, Z.; Wang, W.; Lu, A.; Wu, Y.; Liu, Y.; Yan, C.; Han, C. Rapid Classification of Honey Varieties by Surface Enhanced Raman Scattering Combining with Deep Learning. In Proceedings of the 2018 Cross Strait Quad-Regional Radio Science and Wireless Technology Conference (CSQRWC), Xuzhou, China, 21–24 July 2018; IEEE: Piscataway, NJ, USA, 2018; p. 18092502.

256. Sha, P.; Dong, P.; Deng, J.; Wu, X. Rapid Identification and Quantitative Analysis of Anthrax Protective Antigen Based on Surface-Enhanced Raman Scattering and Convolutional Neural Networks. In *2021 IEEE 21st International Conference on Nanotechnology (NANO)*; IEEE: Piscataway, NJ, USA, 2021; pp. 155–158.

257. Paryanti, G.; Faig, H.; Rokach, L.; Sadot, D. A Direct Learning Approach for Neural Network Based Pre-Distortion for Coherent Nonlinear Optical Transmitter. *J. Light. Technol.* **2020**, *38*, 3883–3896. [CrossRef]

258. Lee, G.-G.C.; Haung, K.-W.; Sun, C.-K.; Liao, Y.-H. Stem Cell Detection Based on Convolutional Neural Network via Third Harmonic Generation Microscopy Images. In *2017 International Conference on Orange Technologies (ICOT)*; IEEE: Piscataway, NJ, USA, 2017; pp. 45–48.

259. Gupta, A.K.; Hsu, C.-H.; Lai, C.-S. Enhancement of the Au/ZnO-NA Plasmonic SERS Signal Using Principal Component Analysis as a Machine Learning Approach. *IEEE Photonics J.* **2020**, *12*, 20013846. [CrossRef]

260. Rajput, S.K.; Nishchal, N.K. Fresnel Domain Nonlinear Optical Image Encryption Scheme Based on Gerchberg–Saxton Phase-Retrieval Algorithm. *Appl. Opt.* **2014**, *53*, 418–425. [CrossRef] [PubMed]

261. Aşırım, Ö.E.; Yolalmaz, A.; Kuzuoğlu, M. High-Fidelity Harmonic Generation in Optical Micro-Resonators Using BFGS Algorithm. *Micromachines* **2020**, *11*, 686. [CrossRef]

262. Bresci, A.; Guizzardi, M.; Valensise, C.M.; Marangi, F.; Scotognella, F.; Cerullo, G.; Polli, D. Removal of Cross-Phase Modulation Artifacts in Ultrafast Pump–Probe Dynamics by Deep Learning. *APL Photonics* **2021**, *6*, 76104. [CrossRef]

263. Wang, L.; Gao, M.; Zhang, Y.; Cao, F.; Huang, H. Optical Phase Conjugation with Complex-Valued Deep Neural Network for WDM 64-QAM Coherent Optical Systems. *IEEE Photonics J.* **2021**, *13*, 21200412. [CrossRef]

264. Shan, M.; Cheng, Q.; Zhong, Z.; Liu, B.; Zhang, Y. Deep-Learning-Enhanced Ice Thickness Measurement Using Raman Scattering. *Opt. Express* **2020**, *28*, 48–56. [CrossRef]

265. Pereira, V.R.; Pereira, D.R.; de Melo Tavares Vieira, K.C.; Ribas, V.P.; Constantino, C.J.L.; Antunes, P.A.; Favareto, A.P.A. Sperm Quality of Rats Exposed to Difenoconazole Using Classical Parameters and Surface-Enhanced Raman Scattering: Classification Performance by Machine Learning Methods. *Environ. Sci. Pollut. Res.* **2019**, *26*, 35253–35265. [CrossRef]

266. Owaki, S.; Nakamura, M. XPM Compensation in Optical Fiber Transmission Systems Using Neural-Network-Based Digital Signal Processing. *IEICE Commun. Express* **2018**, *7*, 31–36. [CrossRef]

267. Yildiz, N.; San, S.E.; Polat, Ö. Light-Scattering Experiments in Dye-Doped Liquid Crystals Both to Determine Crystal Parameters and to Construct Consistent Neural Network Empirical Physical Formulas for Scattering Amplitudes. *Opt. Commun.* **2011**, *284*, 2173–2181. [CrossRef]

268. Owaki, S.; Nakamura, M. Compensation of Optical Nonlinear Waveform Distortion Using Neural-Network Based Digital Signal Processing. *IEICE Commun. Express* **2017**, *6*, 484–489. [CrossRef]

269. Wang, R.; Liang, F.; Lin, Z. Data-Driven Prediction of Diamond-like Infrared Nonlinear Optical Crystals with Targeting Performances. *Sci. Rep.* **2020**, *10*, 3486. [CrossRef] [PubMed]

270. Williamson, I.A.D.; Hughes, T.W.; Minkov, M.; Bartlett, B.; Pai, S.; Fan, S. Reprogrammable Electro-Optic Nonlinear Activation Functions for Optical Neural Networks. *IEEE J. Sel. Top. Quantum Electron.* **2020**, *26*, 18881115. [CrossRef]

271. Khulbe, M.; Kumar, S. Role of Nonlinear Optics in Big Data Transmission and Next Generation Computing Technologies. In *2019 9th International Conference on Cloud Computing, Data Science & Engineering (Confluence)*; IEEE: Piscataway, NJ, USA, 2019; pp. 234–238.

272. Berry, M.E.; McCabe, S.M.; Shand, N.C.; Graham, D.; Faulds, K. Depth Prediction of Nanotags in Tissue Using Surface Enhanced Spatially Offset Raman Scattering (SESORS). *Chem. Commun.* **2022**, *58*, 1756–1759. [CrossRef] [PubMed]

273. Sun, Y.; Dong, M.; Yu, M.; Xia, J.; Zhang, X.; Bai, Y.; Lu, L.; Zhu, L. Nonlinear All-Optical Diffractive Deep Neural Network with 10.6 Mm Wavelength for Image Classification. *Int. J. Opt.* **2021**, *2021*, 6667495. [CrossRef]

274. Xu, L.; Rahmani, M.; Ma, Y.; Smirnova, D.A.; Kamali, K.Z.; Deng, F.; Chiang, Y.K.; Huang, L.; Zhang, H.; Gould, S.; et al. Enhanced Light–Matter Interactions in Dielectric Nanostructures via Machine-Learning Approach. *Adv. Photonics* **2020**, *2*, 1. [CrossRef]

275. Wright, L.G.; Onodera, T.; Stein, M.M.; Wang, T.; Schachter, D.T.; Hu, Z.; McMahon, P.L. Deep Nonlinear Optical Neural Networks Using Physics-Aware Training. In *Conference on Lasers and Electro-Optics*; Kang Tomasulo, S., Ilev, I., Müller, D., Litchinitser, N., Polyakov, S., Podolskiy, V., Nunn, J., Dorrer, C., Fortier, T., Gan, Q., et al., Eds.; Optica Publishing Group: Washington, DC, USA, 2021; p. FF1A.4.

276. Miscuglio, M.; Mehrabian, A.; Hu, Z.; Azzam, S.I.; George, J.; Kildishev, A.V.; Pelton, M.; Sorger, V.J. All-Optical Nonlinear Activation Function for Photonic Neural Networks [Invited]. *Opt. Mater. Express* **2018**, *8*, 3851. [CrossRef]

277. Girija, R.; Anshula; Singh, H. Security-Enhanced Optical Nonlinear Cryptosystem Based on Modified Gerchberg–Saxton Iterative Algorithm. *Optik* **2021**, *244*, 167568. [CrossRef]

278. Singh, P.; Kumar, R.; Yadav, A.K.; Singh, K. Security Analysis and Modified Attack Algorithms for a Nonlinear Optical Cryptosystem Based on DRPE. *Opt. Lasers Eng.* **2021**, *139*, 106501. [CrossRef]

279. Ghiasuddin; Akram, M.; Adeel, M.; Khalid, M.; Tahir, M.N.; Khan, M.U.; Asghar, M.A.; Ullah, M.A.; Iqbal, M. A Combined Experimental and Computational Study of 3-Bromo-5-(2,5-Difluorophenyl) Pyridine and 3,5-Bis(Naphthalen-1-Yl)Pyridine: Insight into the Synthesis, Spectroscopic, Single Crystal XRD, Electronic, Nonlinear Optical and Biological Properties. *J. Mol. Struct.* **2018**, *1160*, 129–141. [CrossRef]

280. Agarwal, N.R.; Lucotti, A.; Tommasini, M.; Chalifoux, W.A.; Tykwinski, R.R. Nonlinear Optical Properties of Polyynes: An Experimental Prediction for Carbyne. *J. Phys. Chem. C* **2016**, *120*, 11131–11139. [CrossRef]

281. Kutz, N. Deep Learning for Control of Nonlinear Optical Systems. In *AI and Optical Data Sciences II*; Kitayama, K., Jalali, B., Eds.; SPIE: Bellingham, WA, USA, 2021; Volume 11703, p. 41.

282. Wu, J.; Li, Z.; Luo, J.; Jen, A.K.-Y. High-Performance Organic Second- and Third-Order Nonlinear Optical Materials for Ultrafast Information Processing. *J. Mater. Chem. C* **2020**, *8*, 15009–15026. [CrossRef]